



# A circadian rhythm-gated subcortical pathway for nighttime-light-induced depressive-like behaviors in mice

Kai An<sup>1,9</sup>, Huan Zhao<sup>2,9</sup>✉, Ying Miao<sup>1,3,4</sup>, Qi Xu<sup>5</sup>, Yu-Fei Li<sup>1</sup>, Yu-Qian Ma<sup>1</sup>, Yi-Ming Shi<sup>1</sup>, Jia-Wei Shen<sup>1</sup>, Jian-Jun Meng<sup>1</sup>, Yong-Gang Yao<sup>3,4,6</sup>, Zhi Zhang<sup>7</sup>, Ju-Tao Chen<sup>1</sup>, Jin Bao<sup>1,6</sup>, Mei Zhang<sup>1,7</sup> and Tian Xue<sup>1,6,7,8</sup>✉

**Besides generating vision, light modulates various physiological functions, including mood. While light therapy applied in the daytime is known to have anti-depressive properties, excessive light exposure at night has been reportedly associated with depressive symptoms. The neural mechanisms underlying this day-night difference in the effects of light are unknown. Using a light-at-night (LAN) paradigm in mice, we showed that LAN induced depressive-like behaviors without disturbing the circadian rhythm. This effect was mediated by a neural pathway from retinal melanopsin-expressing ganglion cells to the dorsal perihabenular nucleus (dpHb) to the nucleus accumbens (NAc). Importantly, the dpHb was gated by the circadian rhythm, being more excitable at night than during the day. This indicates that the ipRGC→dpHb→NAc pathway preferentially conducts light signals at night, thereby mediating LAN-induced depressive-like behaviors. These findings may be relevant when considering the mental health effects of the prevalent nighttime illumination in the industrial world.**

Light is crucial for most species, including humans, to survive and thrive. Besides its obvious role in the generation of vision, light modulates a wide variety of physiological functions such as the biological rhythm, sleep and arousal, cognition and mood<sup>1,2</sup>. During a typical 'solar day', diurnal animals may be exposed to about 12 h of continuous light. In humans, light therapy is widely known to have anti-depressive properties<sup>3–5</sup>, whereas LAN can have negative effects on mood. Exposure to excessive LAN, either from 'sky-glow' or the use of electronic devices such as mobile phones or personal computers before bedtime, has been associated with a greater risk for depressive symptoms<sup>6–10</sup>. These contradicting effects of light during different circadian phases suggest that the timing of light exposure could be a critical factor. Insights into the neural mechanism behind this apparent paradox are fundamental to our understanding of mood regulation by light, but they are yet to be elucidated.

To mammals, light is a potent entraining cue for the circadian rhythm<sup>11</sup>. Hence, light could affect mood indirectly through modulations of the circadian system. Previous investigations have demonstrated that certain forms of LAN can disrupt circadian rhythm at both the molecular and physiological levels<sup>12–14</sup>. Nonetheless, multiple lines of evidence further hint at the presence of a direct neural pathway through which light regulates affective behaviors independent of the circadian deterioration<sup>2,15</sup>. A recent study in mice has implicated the perihabenular nucleus (pHb) in mediating depressive-like effects

induced by a fast ultradian photoperiod (T7 cycle: 3.5 h light and 3.5 h dark)<sup>16</sup>. However, such a fast light/dark cycle typically causes free-running of the circadian rhythm, so that in this T7 protocol light exposure might occur at variable circadian times. Therefore, it is difficult to accurately evaluate the effect of nighttime light exposure on mood-relevant behaviors. We therefore designed a protocol in which light was specifically delivered at night while animals remained entrained to the 12h:12h photoperiod, to enable precise interrogation of the neural circuit mediating LAN-induced depressive-like behaviors, and of the mechanism with which the neural system distinguishes nighttime versus daytime light.

Mammalian light sensation is primarily achieved through retinal photoreceptors. Beyond the image-forming rods and cones, there exists a third group of photoreceptors in the retinae: the intrinsically photosensitive retinal ganglion cells (ipRGCs), which mediate non-image-forming vision. They detect light using melanopsin with a peak sensitivity to blue light (~480 nm wavelength) and convey information regarding ambient irradiance to multiple subcortical nuclei<sup>17–20</sup>. In the current study, we show that LAN-induced depressive-like behaviors require ipRGC projections to pHb and projections from the dpHb to the nucleus accumbens (NAc). In addition, we show that the activity of this ipRGC→dpHb→NAc pathway is gated by the circadian rhythm to preferentially conduct light signals at night and hence specifically mediate the behavioral changes elicited by LAN.

<sup>1</sup>Hefei National Laboratory for Physical Sciences at the Microscale, Neurodegenerative Disorder Research Center, CAS Key Laboratory of Brain Function and Disease, School of Life Sciences, Division of Life Sciences and Medicine, University of Science and Technology of China, Hefei, China. <sup>2</sup>College of Biology, Food and Environment, Hefei University, Hefei, China. <sup>3</sup>Key Laboratory of Animal Models and Human Disease Mechanisms of the Chinese Academy of Sciences and Yunnan Province, Kunming Institute of Zoology, Chinese Academy of Sciences, Kunming, China. <sup>4</sup>KIZ-CUHK Joint Laboratory of Bioresources and Molecular Research in Common Diseases, Kunming Institute of Zoology, Chinese Academy of Sciences, Kunming, China. <sup>5</sup>Department of Physiology, School of Basic Medical Sciences, Anhui Medical University, Hefei, China. <sup>6</sup>Center for Excellence in Brain Science and Intelligence Technology, Chinese Academy of Sciences, Shanghai, China. <sup>7</sup>Eye Center, The First Affiliated Hospital of USTC, Division of Life Sciences and Medicine, University of Science and Technology of China, Hefei, China. <sup>8</sup>Institute for Stem Cell and Regeneration, Chinese Academy of Sciences, Beijing, China. <sup>9</sup>These authors contributed equally: Kai An, Huan Zhao. ✉e-mail: [hzhao@hfuu.edu.cn](mailto:hzhao@hfuu.edu.cn); [xuetian@ustc.edu.cn](mailto:xuetian@ustc.edu.cn)

## Results

**Mice subjected to LAN exhibit depressive-like behaviors.** To assess the behavioral effects of exposure to nighttime light, we established a murine LAN paradigm in which mice were exposed to 2 h of blue light (~400 lux) between zeitgeber time (ZT) 13 and ZT 15. Control animals were exposed to identical total illumination with 2 h of blue light applied between ZT 1 and ZT 3, referred to as the 'light in daytime' (LID) group (Fig. 1a). Wild-type mice (WT; Fig. 1b) exposed to LAN exhibited depressive-like phenotypes (Fig. 1h–i), including increased immobility in the forced swimming test (FST, Fig. 1h and Extended Data Fig. 1h) without changes in overall locomotor activities (Extended Data Fig. 1g), and decreased preference in the sucrose preference test (SPT, Fig. 1i), without altered total consumption (Extended Data Fig. 1i). Such a LAN effect appeared to be dose dependent, for it took at least 3 weeks for animals to progressively develop depressive-like phenotypes, and 3 weeks was therefore chosen as the standard length of our LAN or LID exposure (Extended Data Fig. 1b). We also found that the depressive-like behaviors could last over 3 weeks following the termination of LAN (Extended Data Fig. 1c,d). On the other hand, 3-week exposure to the regular photoperiod with identical total illumination (LID) did not alter behavior in these tests (Figs. 1d,e and Extended Data Fig. 1i). Daytime light is assumed not to disturb circadian rhythm; in fact, neither LID nor LAN altered the general circadian rhythmicity of the animals as indicated by their wheel-running activities (Fig. 1c for LID and Fig. 1g for LAN) and by their rhythmic expression of Period 1 (Per1) protein (an essential element in the endogenous rhythm<sup>21,22</sup>) in the suprachiasmatic nucleus (SCN) (Fig. 1f and Extended Data Fig. 1a).

Because ipRGCs are known to mediate several non-image-forming visual functions, we examined the involvement of ipRGCs in LAN effects. Melanopsin-only (MO) mice (*rd1/rd1;cDTA*), which lack rods/cones but have normal ipRGC-mediated photoreception (Fig. 1j), were subjected to LAN. After 3 weeks of LAN, the MO mice showed increased immobility in the FST (Fig. 1l), and reduced preference for sucrose compared to pre-LAN (Fig. 1m and Extended Data Fig. 1i). By contrast, LAN had no effects in mice with ipRGC ablation and intact rod/cone photoreceptors

(DTA; *Opn4-cre;Rosa-DTA*; see Methods for details; Fig. 1n–q, and Extended Data Fig. 1e,f,i), suggesting that ipRGCs, rather than the conventional image-forming visual pathway were required for the effects of LAN. Both MO and DTA mice remained entrained to the photoperiods (Fig. 1k,o). By contrast, mice with total blindness (triple knock out (TKO); *rd1/rd1;cDTA;Opn4<sup>-/-</sup>*; Fig. 1r), although engaging in wheel-running activities less than WT mice as observed by us and others<sup>23,24</sup>, exhibited 'free-running' of circadian rhythm due to the lack of photoreception (Fig. 1s) and were not affected by LAN exposure (Fig. 1t,u and Extended Data Fig. 1i). These results show that LAN, but not LID, can induce depressive-like phenotypes without affecting the circadian rhythm, and ipRGCs play a necessary and sufficient role in mediating the LAN effects on mood-relevant behaviors.

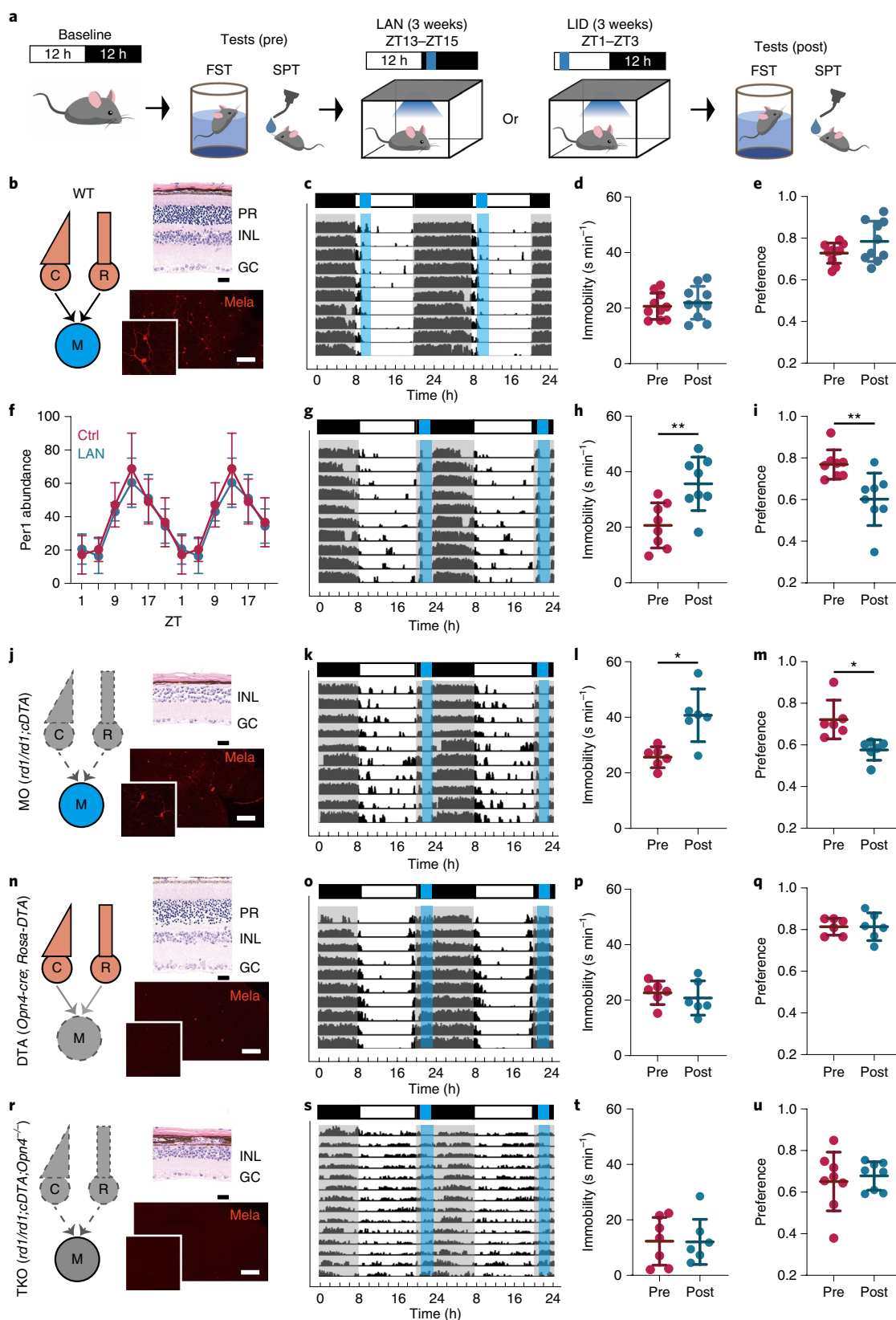
**The pHb receives projection from ipRGCs and is required for the LAN effect.** Next, we sought to delineate the central nucleus (or nuclei) that mediated the LAN effect. Anterograde tracing experiments (Extended Data Fig. 2a) using Alexafluor 555-conjugated cholera toxin subunit B (CTB-555) or herpes simplex virus (HSV-129) confirmed retinal projections to the pHb (Extended Data Fig. 2b,b<sup>''</sup>). Specific labeling of ipRGC axonal terminals was also observed in the pHb area (Extended Data Fig. 2b<sup>''</sup>) as previously reported<sup>20</sup>. We then conducted retrograde tracing experiments (Extended Data Fig. 2c,g) and revealed that retinal innervation of the pHb arose predominantly from M1 ipRGCs in the contralateral eye (Extended Data Fig. 2d–f), with dendrites stratified solely in the OFF sublamina of the retinal inner plexiform layer (Extended Data Fig. 2d), along with a few M2 subtypes (Extended Data Fig. 2h), M3 subtypes (Extended Data Fig. 2i) and displaced ipRGCs (Extended Data Fig. 2j).

Excitotoxic lesion of the pHb (Fig. 2a,b) abolished LAN-induced depressive-like phenotypes (Fig. 2c,d and Extended Data Fig. 3b), implying an essential role of the pHb in the LAN effect. This is in line with our behavioral data that ipRGC-ablated animals (DTA mice) were insensitive to LAN. In those animals, retinal projections to the pHb were entirely absent (Extended Data Fig. 1e); however,

**Fig. 1 | Mice subjected to LAN exhibit depressive-like behaviors.** **a**, Experimental design for LAN or LID paradigms. Identical illumination (same intensity and length) was used for LAN and LID. **b**, Left: schematic illustration of a WT retina with intact rods (R), cones (C) and ipRGCs (M). Right: hematoxylin and eosin (HE) staining of retinal cross-sections (PR, photoreceptor; INL, inner nuclear layer; GC, ganglion cell) and melanopsin immunoreactivity (mela) on a flat-mounted retina showing the presence of all three types of photoreceptors. **c**, Double-plotted actogram showing wheel-running activities of WT mice under LID conditions. **d**, The immobility (immobile time per minute, mean  $\pm$  s.d.) of the mice in the FST test before (pre) and after (post) LID exposure was not statistically different ( $n=10$  mice,  $P=0.2248$ ), as determined by two-tailed paired  $t$ -test. **e**, The preference for sucrose (amount of sucrose consumed/total water intake in 24 h, mean  $\pm$  s.d.) of the mice pre and post the LID exposure was not altered ( $n=10$  mice,  $P=0.1495$ , two-tailed paired  $t$ -test). **f**, Relative abundance of the Per1 protein in the SCN (mean  $\pm$  s.d.) of control (ctrl, pink) and LAN-exposed (LAN, blue) mice. Abundance of Per1 was quantified as number of Per1 immunoreactive cells in the SCN by the same investigator, and normalized to the peak value of ZT 13 in the ctrl group. For both groups,  $n=4, 4, 3, 3, 3$  and 3 mice at ZT 1, 5, 9, 13, 17 and 21, respectively. Two-way ANOVA interaction  $F(5, 28)=0.3554$ ,  $P=0.8744$ . **g**, Wheel-running activities of WT mice under LAN conditions. **h**, Immobility time (mean  $\pm$  s.d.) of WT mice in FST was significantly elevated after LAN exposure ( $n=8$  mice,  $P=0.0019$ ,  $t=4.839$  d.f. = 7, two-tailed paired  $t$ -test). **i**, Sucrose preference (mean  $\pm$  s.d.) of WT mice in SPT was significantly lowered after LAN exposure ( $n=8$  mice,  $P=0.0033$ ,  $t=4.363$  d.f. = 7, two-tailed paired  $t$ -test). **j**, Left: schematic illustration of a melanopsin-only (MO) retina with degenerated rods and cones, but intact ipRGCs. Right: HE staining showing degenerated PR layer of the retina and melanopsin immunostaining showing the presence of functional ipRGCs. **k**, Wheel-running of MO mice under LAN conditions. **l**, Immobility time (mean  $\pm$  s.d.) of LAN-exposed MO mice was significantly elevated ( $n=6$  mice,  $P=0.0365$ ,  $t=2.834$  d.f. = 5, two-tailed paired  $t$ -test). **m**, Sucrose preference (mean  $\pm$  s.d.) of LAN-exposed MO mice was significantly decreased ( $n=6$  mice,  $P=0.0134$ ,  $t=3.741$ , d.f. = 5, two-tailed paired  $t$ -test). **n**, Left: schematic illustration of a DTA retina with normal rods and cones, but lacking ipRGCs. Right: HE staining showing normal PR layer of the retina and melanopsin immunostaining showing the absence of ipRGCs. **o**, Wheel-running of DTA mice under LAN conditions. **p,q**, Immobility (mean  $\pm$  s.d.) in FST (**p**) and sucrose preference (mean  $\pm$  s.d.) in SPT (**q**) of DTA mice, respectively, were not altered by LAN exposure ( $n=6$  mice,  $P=0.3805$  for FST and  $0.9938$  for SPT, respectively, both by two-tailed paired  $t$ -test). **r**, Left: schematic illustration of a TKO retina with degenerated rods and cones, and nonphotoreceptive ipRGCs. Right: HE staining showing degenerated PR layer of the retina and melanopsin immunostaining showing the absence of melanopsin (thus ipRGCs were not photoreceptive). **s**, Actogram showing that the rhythm of TKO mice was 'free-running' without light-entrainment (under LAN conditions). **t,u**, Neither immobility time (mean  $\pm$  s.d.) in FST (**t**) nor preference (mean  $\pm$  s.d.) in SPT (**u**) of TKO mice was altered by LAN exposure ( $n=7$  mice,  $P=0.9421$  for FST;  $n=8$  mice,  $P=0.6480$  for SPT, respectively, both by two-tailed paired  $t$ -test). \* $P<0.05$ ; \*\* $P<0.01$ . Scale bars, 25  $\mu$ m in HE-stained images and 200  $\mu$ m in melanopsin-stained images. HE staining and melanopsin staining for each group were independently repeated three times.

they remained entrained to the photoperiod, probably due to a small fraction of spared retinal innervation to the SCN (Extended Data Fig. 1f). We then selectively expressed the light-sensitive ion channel channelrhodopsin 2 (ChR2) in ipRGCs (Fig. 2e and Extended Data Fig. 3a) using the Cre-loxP system driven by the *Opn4* (*Opn4*, gene

ID 30044, encoding melanopsin) promoter to assess the physiological relevance of the ipRGC–pHb projection. The synaptic transmission from ipRGCs onto pHb neurons was electrophysiologically verified in vitro ( $n = 8$ , Fig. 2f), and was sensitive to a cocktail of glutamatergic blockers (20  $\mu\text{M}$  6-cyano-7-nitroquinoxaline-2,3-dione



(CNQX) + 20  $\mu$ M 2-amino-5-phosphonovaleric acid (APV)). Optostimulation of ipRGC terminals in vivo markedly upregulated cFos expression within or near the pHb (Extended Data Fig. 3c). More importantly, in support of the potential involvement of this pathway in LAN-induced negative mood, acute activation of ipRGC–pHb projections at night elicited strong anhedonia in behaving animals (Fig. 2g and Extended Data Fig. 3b), although it did not affect immobility in the tail suspension test (TST, Fig. 2h). Interestingly, similar optogenetic manipulation during the daytime did not affect the sucrose preference (Fig. 2i).

**ipRGCs innervate dpHb and ventral pHb (vpHb) subpopulations that project to NAc and medial prefrontal cortex (mPFC), respectively.** To identify the downstream projections of ipRGC-innervated pHb neurons, we employed AAV1-Cre, a viral tool with anterograde trans-synaptic spread properties<sup>25</sup>. Intravitreal injection of AAV1-Cre combined with AAV-DIO (double-floxed inverted open reading frame)-eGFP (enhanced GFP) delivered into the pHb (Fig. 2j) resulted in Cre-inducible expression of green fluorescence in ipRGC-recipient pHb neurons (Fig. 2k), which were mainly GABA immunoreactive (Fig. 2l,m). We found the most intense labeling of the GFP<sup>+</sup> axonal terminals in the NAc, a reward associated brain region<sup>26,27</sup> (Fig. 2n), along with sparse signals in the mPFC (Fig. 2o,p, with quantifications in Fig. 2q). Simultaneous retrograde tracing from mPFC and NAc, using the CTB-555 and retroAAV-Cre/DIO-GFP system, respectively (Fig. 2r,s), unveiled two segregated populations of neurons, with the dpHb neurons mainly projecting to the NAc and the vpHb neurons mainly projecting to the mPFC (Fig. 2t,u, quantification in Fig. 2v). Tracing experiments with the combined use of CTB-555 and CTB-488 yielded highly consistent

results (Extended Data Fig. 3d–f), evidently demonstrating the distinct projection patterns of the dpHb versus vpHb.

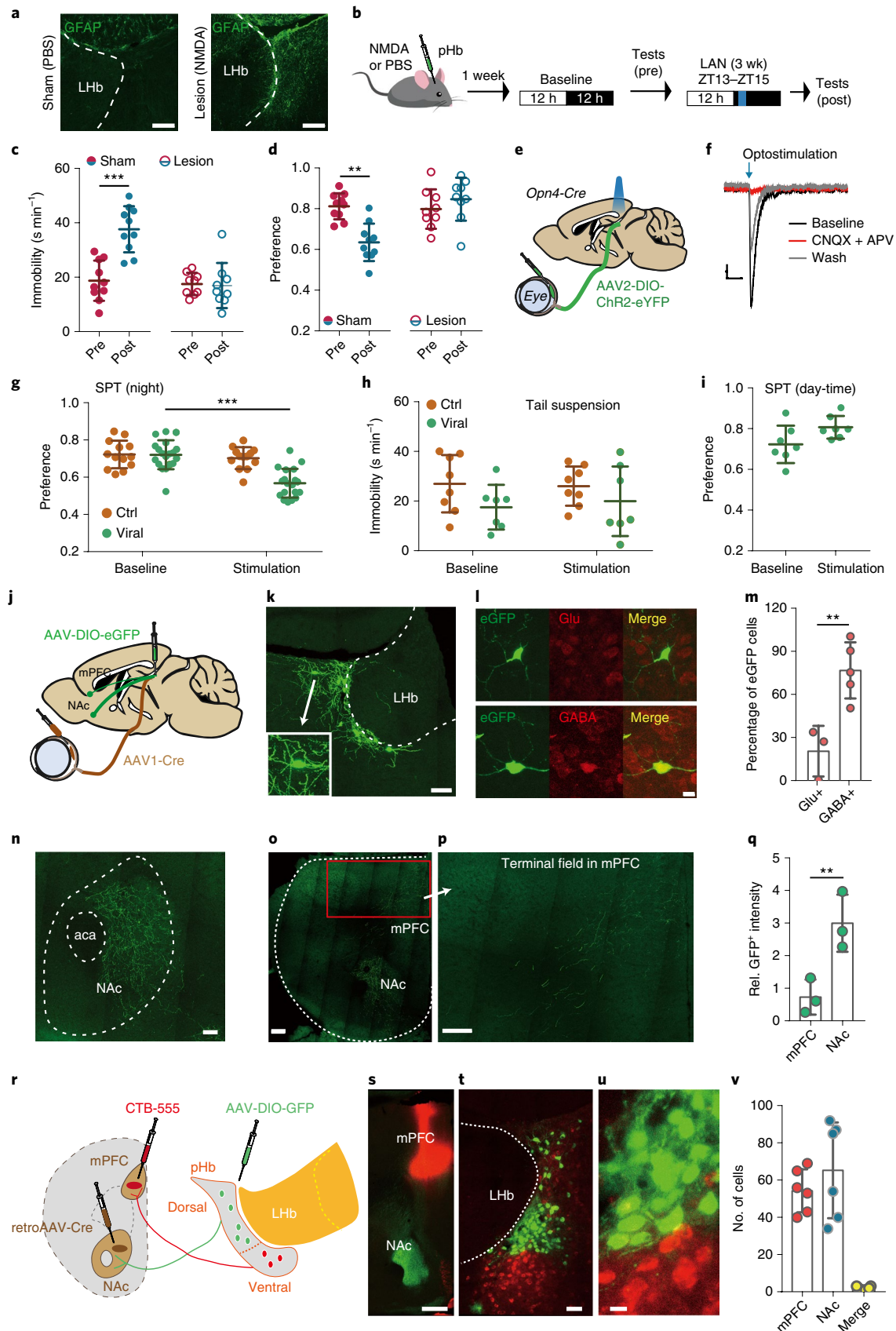
**dpHb and vpHb neurons are differentially modulated by the circadian rhythm.** To investigate why LAN, but not regular daylight, caused depressive-like behaviors in mice, we closely examined the pHb since it was the link between light inputs and the mood centers. We recorded the electrophysiological properties of dpHb and vpHb neurons that were projecting to NAc and mPFC, respectively, at different circadian times on freshly prepared brain slices. During the night, NAc-projecting dpHb neurons (Fig. 3a) were capable of sustaining spiking activities when injected with depolarizing currents (Fig. 3b,e), whereas during the day, the same amount of injected current failed to evoke sustaining spikes in these neurons (Fig. 3b,e). By contrast, the excitability of mPFC-projecting vpHb neurons (Fig. 3h) was similar at night and during the day (Fig. 3i,j). This suggests that the circadian rhythm gates the excitability of NAc-projecting dpHb neurons but not mPFC-projecting vpHb neurons. Further interrogation revealed that 3 weeks of LAN exposure reduced, but did not abolish, the circadian variation in the intrinsic excitability of NAc-projecting dpHb neurons (Fig. 3f,g, in comparison with day versus night from Fig. 3e).

Such gating of neuronal excitability could be controlled by the particular circadian phase or determined by the presence/absence of the light. We thus further interrogated the system by applying ‘dark/day’ and ‘light/night’ conditions (Fig. 3c). Under ‘dark/day’ conditions, mice that had been maintained under regular 8:00 to 20:00 photoperiods were kept in the dark after 8:00 for one additional hour right before preparation for brain slice recordings, and were thus in the circadian day but without light input. Likewise,

**Fig. 2 | LAN effect requires the pHb, which is innervated by ipRGCs and projects to NAc and mPFC via distinct subpopulations of neurons.** **a**, Verification of NMDA lesion using GFAP (green) staining. Staining was performed in all ten mice in the sham group and ten mice in the lesion group, with one removed from further analysis due to incomplete lesion. Scale bars, 100  $\mu$ m. Animals in the sham group were parallel-operated on and injected with equal volumes of PBS. **b**, Experimental design for assessment of LAN effect on mice with excitotoxic lesion of the pHb area. **c**, The immobility time (mean  $\pm$  s.d.) in the FST of mice with pHb lesion (open circles) or sham-operated controls (solid circles) before (pre, pink) and after (post, blue) the LAN exposure. For the sham group,  $n=10$  mice,  $P=0.0008$ , two-tailed paired  $t$ -test; for the lesion group,  $n=9$  mice,  $P=0.8710$ , two-tailed paired  $t$ -test. **d**, The preference for sucrose (mean  $\pm$  s.d.) of mice with pHb lesion or sham controls before and after the LAN exposure. For the sham group,  $n=10$  mice,  $P=0.0031$ , two-tailed paired  $t$ -test; for the lesion group,  $n=9$  mice,  $P=0.2495$ , two-tailed paired  $t$ -test. **e**, Scheme of optogenetic activation of ipRGC terminals within the pHb. AAV2-DIO-ChR2-eYFP (enhanced YFP) was intravitreally injected into the eyes of *Opn4-cre* mice to selectively express ChR2 in ipRGCs. **f**, Representative traces of postsynaptic currents elicited by optostimulation (blue arrow, 5 ms) recorded from a pHb neuron on a brain slice preparation. The red trace was recorded with 20  $\mu$ M APV and 20  $\mu$ M CNQX added to the bath. Scale bars, 10 pA and 20 ms. **g**, Optogenetic stimulation of ipRGC projections to the pHb in vivo markedly suppressed the preference for sucrose (mean  $\pm$  s.d.) in experimental mice (viral,  $n=19$  mice, green, baseline versus stimulation  $P<0.0001$ ,  $t=6.171$ , d.f.=18, two-tailed paired  $t$ -test) but not in the control group (without virus injections,  $n=13$  mice, brown,  $P=0.3731$ ). **h**, Acute optogenetic activation of ipRGC terminals in the pHb did not alter the immobility (mean  $\pm$  s.d.) in TST. The immobility durations of *Opn4-cre* mice that received intravitreally administered AAV2/2-EF1 $\alpha$ -DIO-ChR2-eYFP (viral,  $n=7$  mice, green,  $P=0.6043$ ), as well as control animals (ctrl,  $n=8$  mice, brown,  $P=0.8333$ ) were not statistically altered upon optostimulation (stimulation) delivered through an optic fiber implanted into the pHb in comparison to the baseline immediately before the stimulation. **i**, Optogenetic stimulation of ipRGC terminals in the pHb during the daytime failed to suppress the sucrose preference (mean  $\pm$  s.d.) in ChR2-expressing experimental animals ( $n=7$  mice,  $P=0.1222$ , two-tailed paired  $t$ -test). **j**, Schematic diagram of anterograde trans-synaptic tracing. Intravitreal AAV1-Cre was combined with Cre-inducible eGFP delivered into the pHb. All tracing experiments were repeated at least three times. **k**, GFP-expressing ipRGC-innervated neurons (close-up view shown in inset) in the pHb. Scale bar, 100  $\mu$ m. The tracing experiment was independently repeated at least three times. **l**, GFP<sup>+</sup> neurons in pHb, as shown in **k**, were primarily GABA immunoreactive (bottom row, repeated five times) but rarely colocalized with glutamate (Glu) immunoreactivity (top row, repeated three times). Scale bar, 20  $\mu$ m. **m**, Quantification (mean  $\pm$  s.d.) of the percentages of GFP<sup>+</sup> cells that were GABA or Glu immunoreactive. GABA,  $n=5$  mice (25 sections); Glu,  $n=3$  mice (12 sections);  $P=0.0095$ ,  $t=4.193$ , d.f.=4.755, two-sided unpaired  $t$ -test with Welch's correction. **n**, Terminal field of ipRGC-innervated pHb neurons in the NAc. Aca, anterior commissure, anterior part. Scale bar, 100  $\mu$ m. **o,p**, Terminal field of ipRGC-innervated pHb neurons in the mPFC and close-up view. Scale bar, 200  $\mu$ m. Experiments in **n–p** were independently repeated three times. **q**, Projection intensities of ipRGC-innervated pHb neurons to the NAc and mPFC (based on experiments in **j,k**). Relative (Rel.) density of the axonal terminals was quantified as the green fluorescent intensity over background in a unit area using ImageJ software and presented as mean  $\pm$  s.d. Data for NAc and mPFC were collected from the same sections ( $n=3$  mice for 7 sections).  $P=0.0075$ ,  $t=11.5$ , d.f.=2, two-tailed paired  $t$ -test. **r**, Schematic diagram of simultaneous retrograde tracing from NAc and mPFC. RetroAAV-Cre was injected into the NAc to express Cre recombinase in the NAc-projecting dpHb neurons, which were then labeled with Cre-dependent expression of GFP. CTB-555 was injected into the mPFC. **s**, Fluorescence at the injection sites: mPFC (red) and NAc (green). Scale bar, 500  $\mu$ m. **t,u**, Retrogradely labeled NAc-projecting dpHb neurons (green) and mPFC-projecting vpHb neurons (red) with rare overlaps (yellow). Scale bars, 50  $\mu$ m in **t** and 10  $\mu$ m in **u**. Experiments in **s–u** were independently repeated six times. **v**, Quantification (mean  $\pm$  s.d.) of labeled dpHb versus vpHb neurons in **r** ( $n=6$  mice). \*\* $P<0.01$ ; \*\*\* $P<0.001$ .

mice in the 'light/night' group were kept in room light after 20:00 on the day of the experiment, being in the circadian night but with light input. Our results demonstrated that the mere presence of

light did not reverse the spiking properties of NAc-projecting dpHb neurons from 'night-like' to 'day-like' (Fig. 3b). Similarly, in the dark/day group, the lack of light input did not reverse the day-like



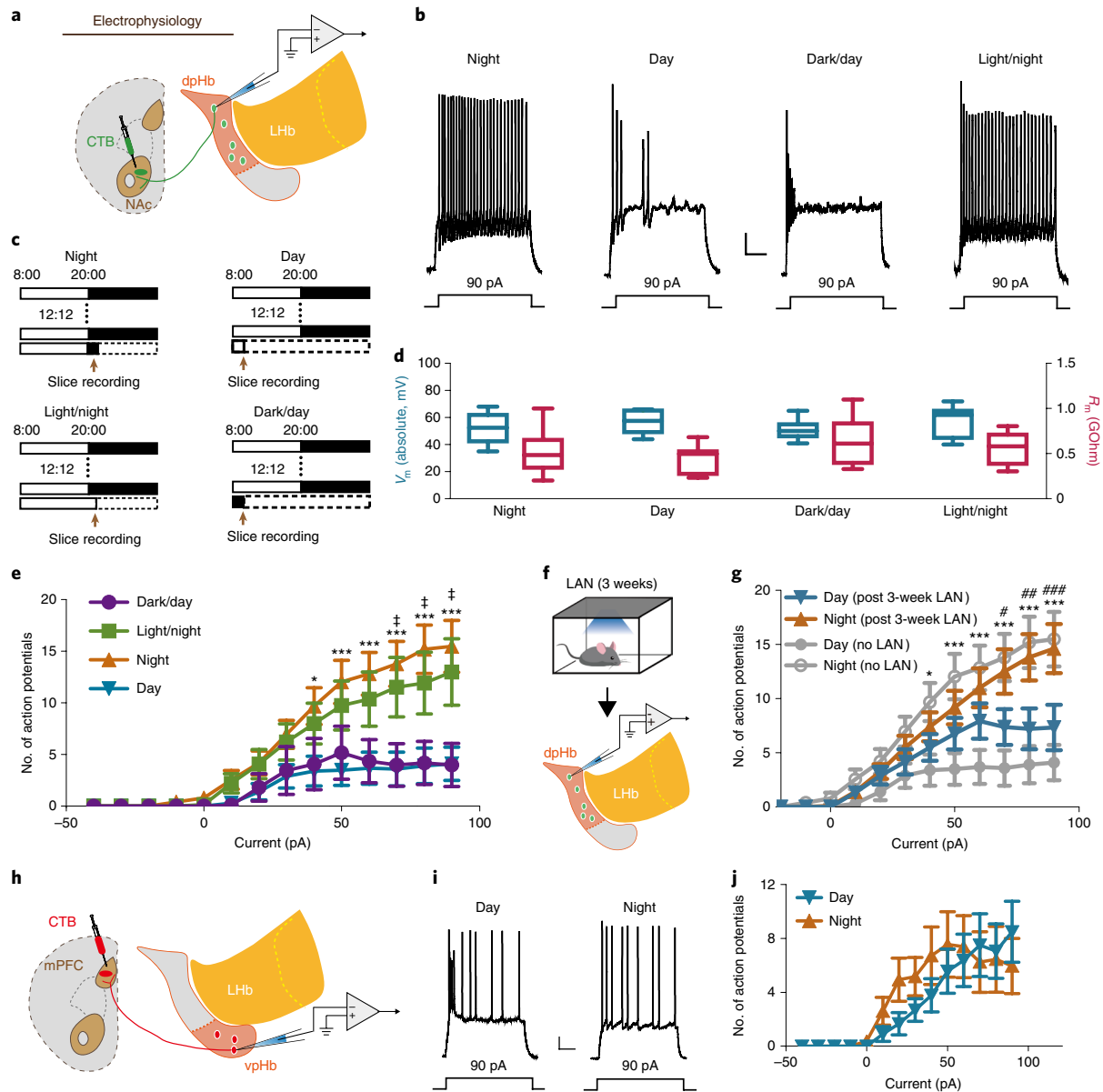


**Fig. 3 | dpHb and vpHb neurons are differentially modulated by the circadian rhythm.** **a**, Schematic diagram of electrophysiological recording selectively on NAc-projecting dpHb neurons. **b**, Spiking patterns of NAc-projecting dpHb neurons in response to a 90-pA current injection during the night, day, dark/day, or light/night (see **c** and text). Scale bars, 10 mV and 200 ms. **c**, Schemes showing light conditions for animals in different groups, which were all housed under normal 12 h:12 h photoperiods until the day of the experiment, and killed at the arrow for acute brain slice preparation. **d**, The resting membrane potential ( $V_m$ , in absolute values, blue) and membrane resistance ( $R_m$ , pink) for each group in **c** were not statistically different among groups (for analyses in **d** and **e**: day,  $n=10$  neurons from 3 mice; night,  $n=20$  neurons from 5 mice; dark/day, 11 neurons from 4 mice; light/night, 13 neurons from 4 mice). One-way ANOVA,  $P=0.2071$ ,  $F(3, 50) = 1.575$ , for  $V_m$ ; and  $P=0.2608$ ,  $F(3, 50) = 1.376$ , for  $R_m$ . The box is plotted at the median extending from the 25th to the 75th percentile, and the whisker represents minimum-to-maximum distribution. **e**, Quantification (mean  $\pm$  s.e.m.) of action potentials generated by current injections in NAc-projecting dpHb neurons. Two-way ANOVA with Bonferroni's test: day versus night,  $F(13, 392) = 3.798$ ,  $P < 0.0001$ , different at 50–90 pA; dark/day versus day,  $P > 0.9999$ ,  $F(13, 266) = 0.05961$ ; light/night versus night,  $P = 0.9980$ ,  $F(13, 434) = 0.2268$ ; dark/day versus light/night,  $F(1, 308) = 23.27$ ,  $P < 0.0001$ . \* indicates 'Day' significantly different from 'Night',  $P < 0.05$ ; \*\*\* indicates 'Day' significantly different from 'Night',  $P < 0.001$ ; ‡ indicates 'Light/night' significantly different from 'dark/day'. **f**, Diagram showing electrophysiological recordings of NAc-projecting dpHb neurons after animals were exposed to LAN for 3 weeks. **g**, Circadian variations in the intrinsic excitability of NAc-projecting dpHb neurons after 3-week LAN exposure. Data were presented as mean  $\pm$  s.e.m.;  $n=18$  neurons from 4 mice for 'Day (post 3-week LAN)' and 22 neurons from 5 mice for 'night (post 3-week LAN)'. Two-way ANOVA:  $F(14, 570) = 2.181$ ,  $P = 0.0075$ , different at 70–90 pA as determined by Sidak's test, \* $P = 0.045$ , \*\* $P = 0.0021$  and \*\*\* $P = 0.0004$ , respectively. Data of 'Day (no LAN)' and 'Night (no LAN)' were replotted from **e** in light gray for easy comparison. Difference between Day (no LAN) and Night (no LAN) is annotated by \* and \*\*\* as in **e**. **h**, Schematic diagram of electrophysiological recording selectively on mPFC-projecting vpHb neurons. **i**, Similar spiking patterns of mPFC-projecting vpHb neurons in response to a 90-pA current injection during the day and night. Scale bars, 10 mV and 200 ms. **j**, Quantification (mean  $\pm$  s.e.m.) of action potentials generated by current injections in mPFC-projecting vpHb neurons ( $n=16$  neurons from 4 mice for day and 20 neurons from 5 mice for night,  $F(13, 476) = 0.5863$ ,  $P = 0.8657$  by two-way ANOVA). Data in **e** and **g** were re-analyzed using nested ANOVA and nested  $t$ -test, respectively, to accommodate the dependence of observations obtained from the same object. Detailed results of the nested analysis are provided in Extended Data Fig. 4, and do not alter the interpretation of these data.

phenotype of these neuron (Fig. 3b,e, and Extended Data Fig. 4) to be more 'night-like'. The membrane properties were consistent among all groups (Fig. 3d). These observations indicate that the excitability of NAc-projecting dpHb neurons was primarily gated by the endogenous rhythm rather than by light conditions.

**dpHb–NAc projections, but not vpHb–mPFC projections, mediate the depressive-like behaviors induced by LAN.** We subsequently tested whether suppression of the dpHb–NAc or vpHb–mPFC projections could ameliorate the depressive-like phenotypes induced by LAN. Cre recombinase was first introduced to NAc-projecting pHb neurons using retroAAV-Cre delivered into the NAc, and then one of the following viruses was injected into the pHb: AAV-DIO-Tet-Tox (light chain of tetanus toxin), AAV-DIO-hM4Di or AAV-DIO-mCherry (Fig. 4a,b). Tet-Tox-mediated synaptic suppression of NAc-projecting dpHb neurons prevented LAN-induced depressive-like phenotypes (Fig. 4c,e, and Extended Data Fig. 5a). However, such permanent repression of the dpHb–NAc projection may have nonspecific consequences; we therefore employed hM4Di, a chemogenetic tool selectively activated by clozapine-*N*-oxide (CNO), to achieve temporally controlled inhibition of NAc-projecting dpHb neurons. CNO was intraperitoneally (i.p.) administered daily at 20:30, so that hM4Di-mediated blockade of the dpHb–NAc projection was precisely timed to the onset of LAN (21:00), and NAc-projecting dpHb neurons should regain functionality after the CNO wash-off. Echoing the Tet-Tox results, mice that expressed hM4Di and received daily CNO did not develop depressive-like behaviors after LAN exposure, confirming an indispensable role of the dpHb–NAc projection in the LAN effects (Fig. 4d,f and Extended Data Fig. 5a). To rule out the possible interference from the virus expression or the mere usage of CNO, we prepared control animals that were either expressing mCherry and receiving daily CNO, or expressing hM4Di and receiving daily PBS. As expected, all control mice became depressive-like after LAN exposure (Fig. 4d,f and Extended Data Fig. 5a). These data demonstrate that the neurophysiological activities of NAc-projecting dpHb neurons were required for the development of depressive phenotypes during LAN exposure.

Immunostaining revealed that the majority of NAc-projecting dpHb neurons were GABA positive (Fig. 4g), as were ipRGC-innervated dpHb neurons (Fig. 2l,m). Electrophysiological recordings from NAc neurons with optogenetic activation of the afferent terminals of the dpHb neurons (Fig. 4h) revealed consistent results. The monosynaptic neurotransmission from dpHb neurons onto NAc neurons was mainly GABAergic, nearly completely abolished by the GABA receptor antagonist picrotoxin (PTX, seven of nine neurons, Fig. 4i,j). Glutamatergic neurotransmission was also observed in two of nine neurons examined (Fig. 4k). It has been well established that ipRGCs use glutamate as the major neurotransmitter<sup>28</sup>, and in our *in vitro* optogenetic experiments (Fig. 2f), excitatory postsynaptic currents were consistently observed with photo-activation of ipRGC terminals. This suggests that light excites ipRGC-recipient pHb neurons, which in turn likely generate inhibitory inputs onto the NAc.

In a similar manner, we evaluated the possible involvement of vpHb–mPFC projections in the LAN-induced depressive-like behaviors. The synaptic transmission of mPFC-projecting vpHb neurons were blocked through the retroAAV-Cre/DIO-Tet-Tox system (Fig. 4l), and both experimental and control animals (expressing only mCherry) were subjected to LAN exposure. Blockade of the vpHb–mPFC projection failed to prevent the depressive-like phenotypes induced by LAN (Fig. 4m,n and Extended Data Fig. 5a). Along with the fact that suppression of the dpHb–NAc projection was sufficient to block the LAN effect while the vpHb–mPFC projection remained intact, these data indicate a minimal role of the vpHb–mPFC projection in the LAN-induced depressive-like behaviors.

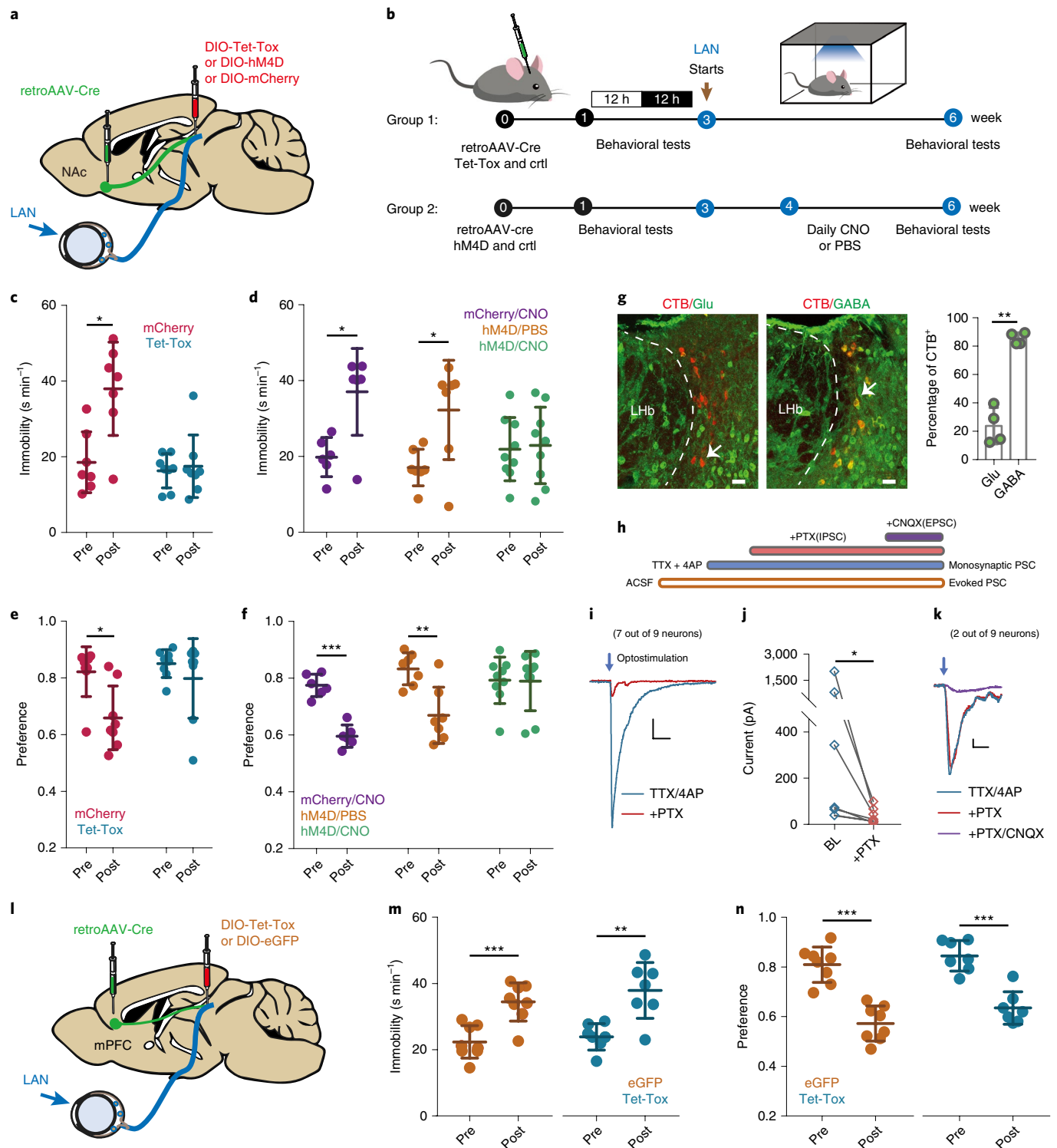
Taken together, our findings revealed that the dpHb–NAc projection and the vpHb–mPFC projection were not only physically segregated and differentially modulated by the circadian rhythm, but were also functionally separated, and that only the dpHb–NAc projection mediated the LAN-induced depressive-like behaviors.

**Light acutely activates pHb–NAc projections, but not vpHb–mPFC projections, under circadian rhythm modulations.** To further verify the synaptic connections between ipRGCs, dpHb and NAc, we conducted retrograde trans-synaptic tracing using modified

**Fig. 4 | dpHb–NAc projection, but not vpHb–mPFC projection, mediates the depressive-like behaviors induced by LAN.** **a**, Experimental strategy for inhibitory manipulations of the dpHb–NAc projection. **b**, Flow diagram of inhibitory manipulations with Tet-Tox (group 1) or hM4D (group 2). For animals in group 2, a daily dose of 1 mg kg<sup>-1</sup> CNO (or equal volume of PBS for controls) was administered at 20:30 via i.p. injection for 14 d consecutively under LAN conditions. **c**, Immobility time (mean ± s.d.) in FST of mice expressing Tet-Tox in NAc-projecting dpHb neurons (Tet-Tox, blue, *n* = 8 mice, *P* = 0.7008, two-tailed paired *t*-test) and control mice expressing only mCherry (mCherry, pink, *n* = 7 mice, *P* = 0.0109, *t* = 3.635, d.f. = 6, two-tailed paired *t*-test). **d**, Immobility time (mean ± s.d.) in FST of mice expressing hM4D and receiving CNO (hM4D/CNO, green, *n* = 9 mice, *P* = 0.7695) and corresponding controls (hM4D/PBS, mice expressing hM4D and receiving PBS, brown, *n* = 7 mice, *P* = 0.0135, *t* = 3.458, d.f. = 6; mCherry/CNO, mice receiving CNO and expressing mCherry, purple, *n* = 6 mice, *P* = 0.0315, *t* = 2.96, d.f. = 5), all by two-tailed paired *t*-test. **e,f**, Preference for sucrose (mean ± s.d.) in the SPT of same animals in **c,d**, respectively. For the Tet-Tox group, *P* = 0.2668; for the mCherry group, *P* = 0.0409, *t* = 2.502, d.f. = 7; for the hM4D/CNO group, *P* = 0.9594; for the hM4D/PBS group, *P* = 0.0015, *t* = 5.543, d.f. = 6; for the mCherry/CNO group, *P* < 0.0001. **g**, GABA or glutamate immunoreactivity (green) in NAc-projecting dpHb neurons retrogradely labeled with CTB-555 (red). Scale bar, 20 μm. Quantification shown on the right as mean ± s.d. GABA+CTB\*: *n* = 4 mice, 45 sections, total of 951 cells; glutamate+CTB\*: *n* = 4 mice, 52 sections, total of 972 cells. Two-sided unpaired *t*-test with Welch's correction: *P* = 0.0013, *t* = 9.133, d.f. = 3.608. **h**, Schematic demonstration of the protocol for patch-clamp recordings. Recordings were made using aCSF as the bath solution and a high-Cl<sup>-</sup> internal solution (see Methods). Monosynaptic inputs from NAc-projecting dpHb neurons were isolated using 100 nM TTX and 40 μM 4AP (blue), and then challenged with 40 μM PTX in the continual presence of TTX and 4AP (+PTX, red). The ones resistant to PTX were challenged with 20 μM CNQX in the continual presence of TTX, 4AP and PTX (+CNQX, purple). **i**, Representative traces of IPSCs elicited by optostimulation (blue arrow, 5 ms) in a NAc neuron on a brain slice preparation. Optogenetically evoked PSC (in TTX/4AP, blue trace) were nearly completely eliminated by 40 μM PTX (+PTX, red trace). Scale bars, 100 pA and 100 ms. **j**, Quantification of the amplitudes of optogenetically evoked currents before (baseline, BL), in the presence of TTX/4AP, blue diamonds) and after (+PTX, red diamonds) PTX application (*n* = 7 of 9 neurons with stable monosynaptic inputs, *P* = 0.0156 by two-sided Wilcoxon matched-pairs signed rank test). **k**, Representative traces of the optogenetically evoked EPSC in 2 of 9 neurons, which were insensitive to 40 μM PTX (+PTX, red) but were abolished by 20 μM CNQX (+PTX/CNQX, purple). Scale bars, 10 pA and 20 ms. **l**, Experimental strategy for inhibitory manipulations of the vpHb–mPFC projection. **m**, The immobility time (mean ± s.d.) of mice with blockage of the vpHb–mPFC projection via Tet-Tox (Tet-Tox, blue, *n* = 7 mice, *P* = 0.0023, *t* = 5.076, d.f. = 6) and control mice expressing only eGFP (eGFP, brown, *n* = 8 mice, *P* = 0.0005, *t* = 6.119, d.f. = 7) were both significantly elevated following LAN exposure, as determined by two-tailed paired *t*-test. **n**, The preference for sucrose (mean ± s.d.) was lowered after LAN exposure in both Tet-Tox and eGFP mice, *P* < 0.0001, *t* = 9.643, d.f. = 6 and *P* = 0.0007, *t* = 5.815, d.f. = 7, respectively, by two-tailed paired *t*-test. \*\**P* < 0.05; \*\*\**P* < 0.01; \*\*\*\**P* < 0.001.

rabies virus (RV-EnvA- $\Delta$ G-dsRed). RetroAAV-Cre was injected into the NAc to infect NAc-projecting dpHb neurons through terminal absorption. Helper viruses (AAV-DIO-RVG to reinstate the trans-synaptic property of RV and AAV-DIO-TVA to facilitate selective infection) were injected into the dpHb (Figs. 5a,b), followed by RV injection 3 weeks later using the same coordinates. After another 2 weeks, on flat-mounted retinae, we found RV-labeled RGCs that were mostly melanopsin positive (Fig. 5c,d), supporting the notion that light could directly activate the dpHb–NAc projection through ipRGCs.

Given the structural evidence of retinal inputs onto dpHb–NAc projection, we next investigated whether light could indeed elicit activation of NAc-projecting dpHb neurons in freely moving animals and, if so, whether such activation was modulated by the circadian rhythm. We hence performed *in vivo* fiber photometry experiments in which calcium recordings were made in freely moving animals exposed to pulses of blue light (Fig. 5e). Selective recordings from NAc-projecting dpHb neurons were achieved through injection of retroAAV-Cre in the NAc combined with AAV-DIO-GCamp6s delivered into the dpHb, and the correct



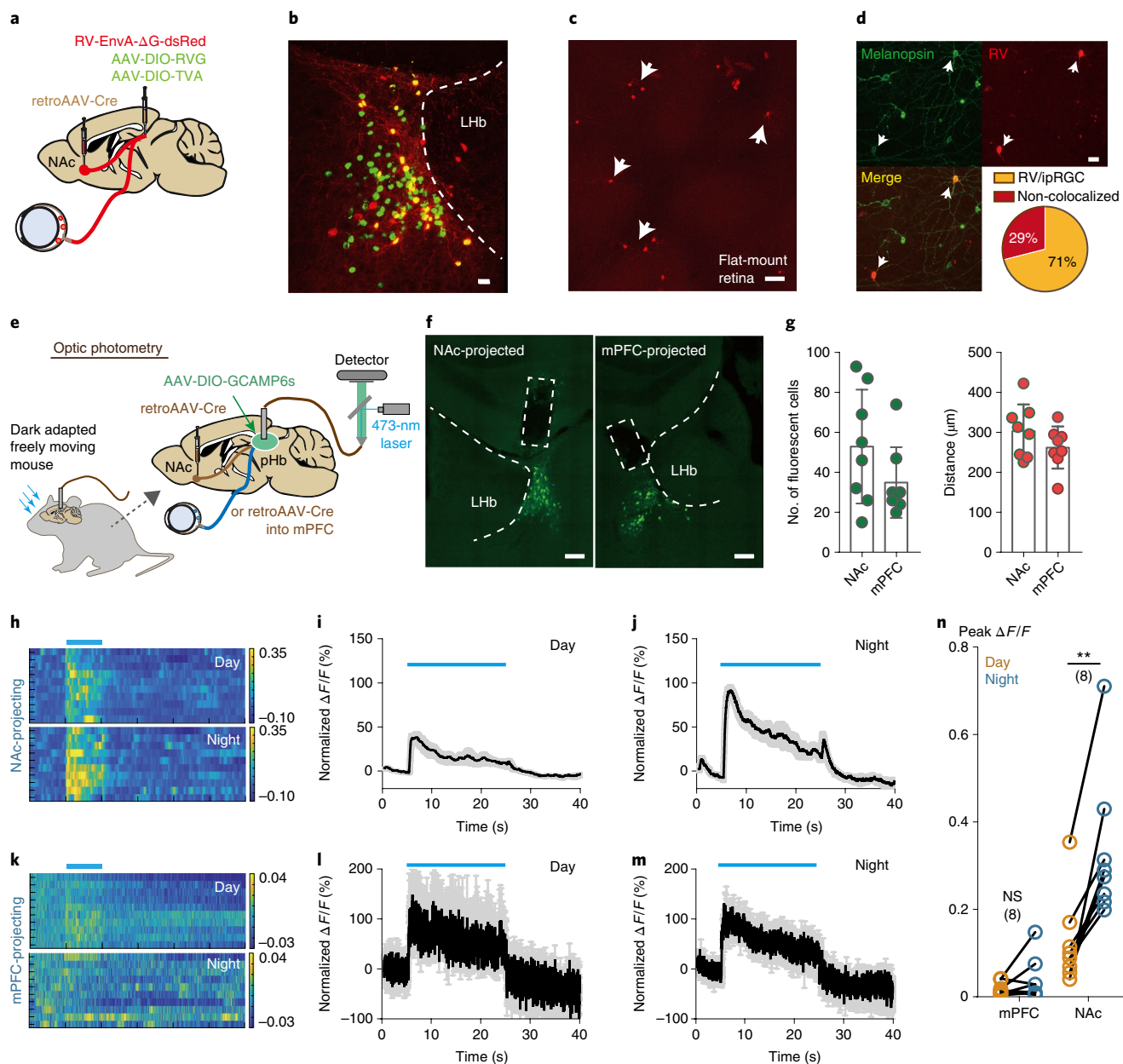


**Fig. 5 | Light acutely activates dHb-NAC projection under circadian modulations.** **a**, Schematic diagram of retrograde trans-synaptic tracing with modified RV system. Tracing in **a–c** as repeated six times. **b**, Starter cells (yellow) in the dHb area (red, RV; green, helper viruses). Scale bar, 20  $\mu\text{m}$ . **c**, RV-labeled (red) RGCs on a flat-mounted retina (arrow heads). Scale bar, 150  $\mu\text{m}$ . **d**, Close-up view showing RV-labeled (red) RGCs colocalized with melanopsin immunoreactivity (green). Scale bar, 20  $\mu\text{m}$ . Quantification of melanopsin positive and negative cells in RV-labeled RGCs ( $n=5$  retinas) revealed that the majority ( $71\% \pm 18\%$ ) of RV-positive RGCs were determined ipRGCs, which is possibly an underestimation due to limited compatibility between RV infection and immunostaining. **e**, Schematic illustration of optic photometry recording from freely moving mice (see Methods for details). **f**, Post hoc examinations verified the correct placement of the optic fiber and sufficient expression of the virus (green) in both NAC-projecting dHb neurons (performed on all 8 clusters from 7 mice) and mPFC-projecting vHb neurons (performed on all 8 clusters from 5 mice). Scale bars, 100  $\mu\text{m}$ . **g**, The infection efficiency (left, quantitated as the number of GCAMP-expressing neurons and expressed as mean  $\pm$  s.d.) and the optical fiber placement (right, quantitated as the distance from the center of the cell cluster to the tip of the optical fiber and expressed as mean  $\pm$  s.d.) were similar in photometric recordings of NAC- and mPFC-projecting pHb neurons, with respective  $P$  values of 0.1555 and 0.1943 determined by two-sided unpaired  $t$ -test with Welch's correction. NAC,  $n=8$  clusters from 7 mice; mPFC,  $n=8$  clusters from 5 mice. **h**, Representative heat maps showing calcium responses elicited by 20 s of blue light (horizontal bar) in a NAC-projecting dHb neuron cluster during the daytime (top) versus at night (bottom). **i, j**, Averaged trace (mean plotted as the black line and s.e.m. as the gray shading) of the light-induced responses of NAC-projecting dHb neuron clusters during the daytime (**i**) versus at night (**j**).  $n=8$  clusters from 7 mice. Individual trace recorded from each cluster was generated by averaging ten trails, then normalized to the peak. **k**, Representative heat maps showing calcium responses of an mPFC-projecting vHb neuron cluster during the daytime (top) versus at night (bottom). **l, m**, Averaged traces (mean plotted as the black line and s.e.m. as the gray shading) of the light-induced responses of mPFC-projecting vHb neuron clusters during the daytime (**l**) and at night (**m**).  $n=8$  clusters from 5 mice. **n**, Comparison of the light elicited responses at night (blue) versus during the day (brown) in both NAC-projecting and mPFC-projecting neurons. For NAC-projecting dHb neuron clusters, peaks at night were statistically greater than peaks during the day,  $P=0.0010$ ,  $t=5.373$ , d.f. = 7, by two-tailed paired  $t$ -test; however, for mPFC-projecting vHb neuron clusters, peaks were statistically nondifferent (NS, not significant),  $P=0.2121$ ,  $t=1.373$ , d.f. = 7. **\*\*** $P < 0.01$ .

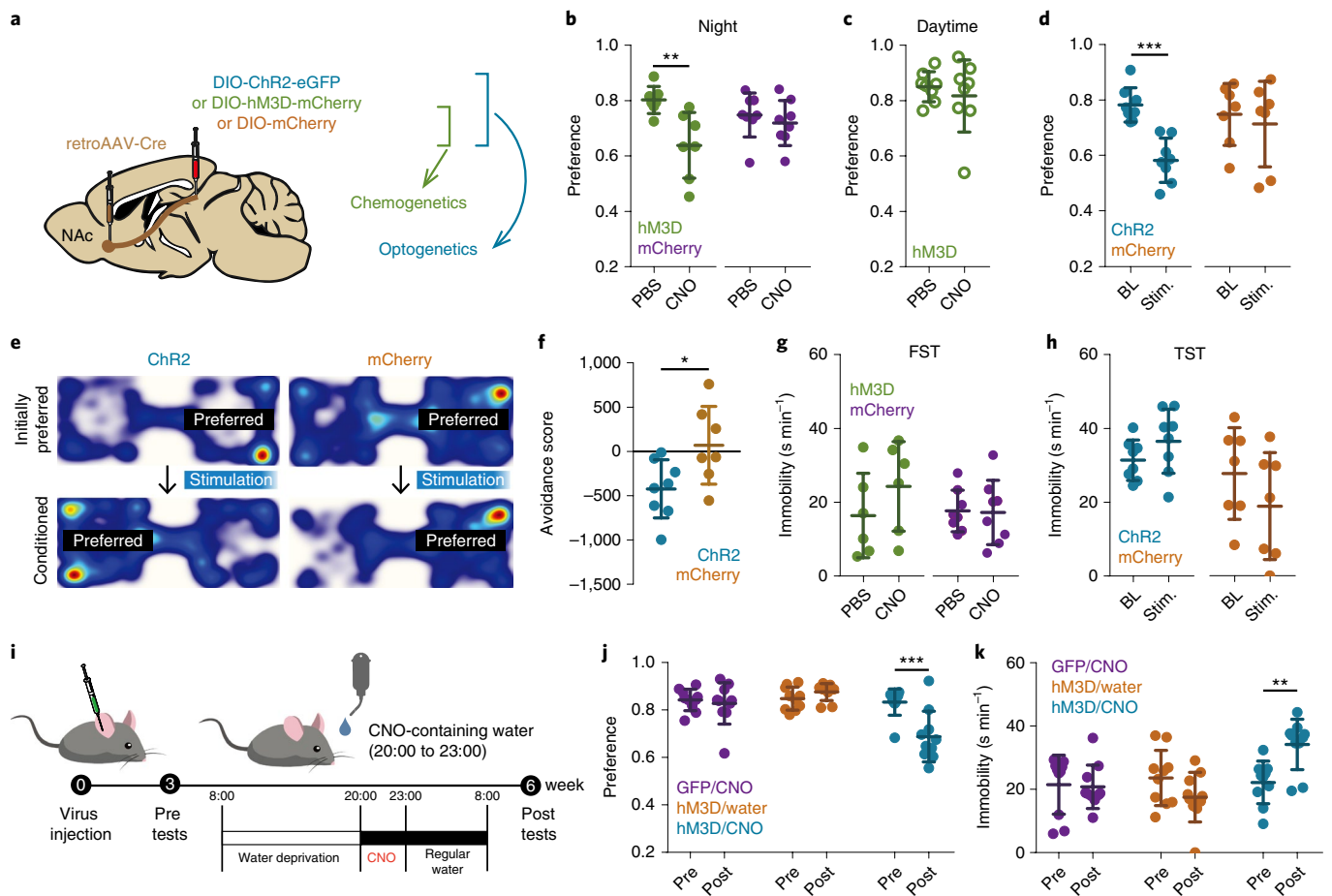


**Fig. 6 | Activation of dpHb-NAc projection induces depressive-like behavioral changes.** **a**, Schematic diagram of optogenetic or chemogenetic activation of NAc-projecting dpHb neurons. **b**, Activation dpHb-NAc projection with hM3D (PBS versus CNO) induced significant anhedonia in mice expressing hM3D selectively in NAc-projecting dpHb neurons (hM3D, green,  $n = 7$  mice,  $P = 0.0061$ ,  $t = 4.13$ , d.f. = 6, two-tailed paired  $t$ -test) but did not affect control mice expressing only mCherry (mCherry, purple,  $n = 8$  mice,  $P = 0.2406$ ). Data were expressed as mean  $\pm$  s.d. **c**, Chemogenetic activation of NAc-projecting dpHb neurons during the daytime did not alter the preference for sucrose (expressed as mean  $\pm$  s.d.,  $n = 8$  mice,  $P = 0.4836$ ,  $t = 0.7396$ , d.f. = 7 by two-tailed paired  $t$ -test). **d**, Optogenetic activation via optostimulation (light stimulation (Stim.) versus BL) reduced sucrose preference in mice with selective expression of ChR2 (ChR2, blue,  $n = 8$  mice,  $P = 0.0009$ ,  $t = 5.495$ , d.f. = 7, two-tailed paired  $t$ -test) but not the controls (mCherry, brown,  $n = 7$  mice,  $P = 0.6995$ ). Data were expressed as mean  $\pm$  s.d. **e**, Heat map showing optostimulation of NAc-projecting dpHb neurons induced RTPA (see Methods). During the test period (conditioned, bottom panels), experimental (ChR2, blue) mice avoided the initially preferred side (top panels) that was coupled with optostimulation; however, place preference of the control (mCherry, brown) mice was not altered. **f**, Avoidance scores (mean  $\pm$  s.d.) calculated from experiments in **e**. A negative value indicated reversal of the place preference.  $n = 7$  mice for mCherry group and  $n = 8$  mice for the ChR2 group,  $P = 0.0335$ ,  $t = 2.427$ , d.f. = 11.03, by two-sided Welch's  $t$ -test. **g**, In FST, acute chemogenetic activation of the NAc-projecting dpHb neurons did not alter the immobility of experimental mice (hM3D, green,  $n = 6$  mice,  $P = 0.2320$  by two-tailed paired  $t$ -test) nor that of the control mice (mCherry, purple,  $n = 8$  mice,  $P = 0.7974$ ). Data were expressed as mean  $\pm$  s.d. **h**, Acute optogenetic activation of NAc-projecting dpHb neurons did not affect the immobility of animals (mean  $\pm$  s.d.) in TST, including both mice with selective ChR2 expression (ChR2, blue,  $n = 8$  mice,  $P = 0.2429$ ) and control animals (mCherry, brown,  $n = 7$  mice,  $P = 0.0871$ ). **i**, Diagram showing the procedures for chronic chemogenetic activation of the pHb-NAc projection (see Methods for details). **j**, Sucrose preference (mean  $\pm$  s.d.) was reduced in animals with selective expression of hM3D and given daily CNO (hM3D/CNO, blue,  $n = 10$  mice,  $P = 0.0009$ ,  $t = 4.886$ , d.f. = 9, two-tailed paired  $t$ -test), but not in control animals receiving daily CNO (GFP/CNO, purple,  $n = 10$  mice,  $P = 0.1893$ ) and hM3D-expressing animal which received only water (hM3D/water, brown,  $n = 10$  mice,  $P = 0.5278$ ). **k**, Consistently, immobility (mean  $\pm$  s.d.) in FST was only elevated in experimental animals (hM3D/CNO,  $P = 0.0017$ ,  $t = 4.405$ , d.f. = 9), but not in both control groups (GPF/CNO,  $P = 0.8478$ ; hM3D/water,  $P = 0.1719$ ), all by two-tailed paired  $t$ -test. \* $P < 0.05$ ; \*\* $P < 0.01$ ; \*\*\* $P < 0.001$ .

placement of the optic fiber was verified by a post hoc examination (Fig. 5f,g). In a parallel manner, we also performed photometric recordings from mPFC-projecting vpHb neurons (Fig. 5f,g). We observed reliable responses of NAc-projecting dpHb neurons to the environment light stimulations (Fig. 5h and Extended Data Fig. 6). Importantly, these neurons exhibited notably greater responses to light stimulations at night than to identical light stimulations during the daytime (Fig. 5i,j,n). By contrast, mPFC-projecting vpHb neurons were not as readily responsive to illumination (Fig. 5k and

Extended Data Fig. 6), and the responses were not statistically different during the daytime versus at night (Fig. 5l-n). Our results confirmed that light could activate the dpHb-NAc projection in behaving animals and the level of activation was governed by the circadian phase.

**Acute activation of dpHb-NAc projections induces anhedonia.** Our previous findings mainly focused on behavioral alterations induced by chronic exposure to LAN. We were thus curious about

the acute effect of LAN-elicited dpHb–NAc neural activation and how it leads to depressive-like states. We employed optogenetic and chemogenetic manipulations to stimulate NAc-projecting dpHb neurons (Fig. 6a and Extended Data Fig. 7a,b). Excitation of these neurons, either by CNO administration or optostimulation, strongly reduced sucrose preference when performed during the night (Fig. 6b,d), yet similar chemogenetic activation during the daytime failed to alter the preference for sucrose (Fig. 6c and Extended Data Fig. 7c). Additionally, in real-time place aversion (RTPA) experiments, optostimulation of NAc-projecting dpHb neurons caused mice to avoid the stimulation-coupled side of the chamber, which was its preferred side during the baseline period. The preference/aversion of mCherry-expressing control mice was not altered as expected (Fig. 6e,f). These results indicate that the acute activation of pHb–NAc projections induce an aversive signal. We speculate that the function of this pathway may be to detect and avoid ‘unusual’ light signals that are off-phase with the circadian rhythm.

Neither chemogenetic (Fig. 6g) nor optogenetic (Fig. 6h) excitation of the dpHb–NAc projection affected immobility in FST and TST, respectively. One possible explanation is that acute activation of the ipRGC–dpHb–NAc pathway primarily causes anhedonia, which—with time and repetitive stimulations—eventually establishes a depressive-like state that manifests as behaviors including decreased sucrose preference and increased immobility in FST or TST. To demonstrate such a possibility, we conducted a long-term experiment with chronic chemogenetic activation of the dpHb–NAc projection, in which animals selectively expressing hM3D in NAc-projecting dpHb neurons were given CNO in drinking water during the period 20:00 to 23:00 for three consecutive weeks (Fig. 6i). Indeed, after 3 weeks, hM3D-expressing animals that received daily CNO, but not animals without hM3D expression or CNO intake, exhibited both decreased sucrose preference and increased immobility in FST (Fig. 6j,k and Extended Data Fig. 7c), similar to the depressive-like behaviors induced by 3 weeks of LAN.

## Discussion

Light pollution is common in modern cities. Sunset is no longer regarded as a signal for the end of the day; rather, many humans now commonly experience an over-illuminated night life, which has raised serious concerns regarding the potentially detrimental biological impacts, on mood in particular<sup>6,7</sup>. As the first step to address this question, we need to identify the neural circuits underlying the influences of LAN on the brain. More importantly, a fundamental question needs to be addressed regarding the neural basis for the divergent effects of light on mood during the day versus at night. In the present study, we identified a circadian-gated ipRGCs–dpHb–NAc pathway that preferentially conducts light at night and that mediates the depressive-like behaviors induced by LAN (see Supplementary Fig. 1, working model). We found that chronic exposure to LAN consistently induced depressive-like phenotypes, which required light-activated ipRGCs and the pHb. The dpHb receives retinal inputs and in turn sends long-range inhibitory neurotransmission to the NAc to induce negative mood. Of note, these dpHb neurons were modulated by the circadian rhythm. Specifically, our *in vivo* and *in vitro* recordings demonstrated that NAc-projecting dpHb neurons were more excitable at night, and hence preferentially responded to LAN but not LID. Our findings in mice thus not only identified a brain pathway responsible for the LAN-induced behavioral changes, but also identified a mechanism that likely contributes to the effects of light on mood-relevant behavior during different circadian phases. The effectiveness of light to induce depressive-like behavior in mice was augmented during the night. Hence it is plausible that although light regulates activities and the sleep/wake cycle in opposite directions in diurnal versus nocturnal animals, when light appears during the ‘wrong’ circadian phase, it may cause depressive-like behaviors in both

nocturnal and diurnal animals by acting through the same ipRGCs–dpHb–NAc pathway.

Our behavioral paradigm enabled us to investigate the direct regulation of behavior by light in a physiologically relevant setting separate from its impact on the circadian rhythm. The immunostaining of Per1 clearly demonstrated that the ‘master clock’ SCN retained its rhythmicity after LAN exposure, and the general rhythm in the wheel-running activities of WT animals under LAN conditions appeared undisrupted. This indicates that the depressive-like phenotypes resulting from LAN exposure were likely attributable to direct effects of light, rather than being a byproduct of the compromised circadian rhythm. In our loss-of-function experiments, blocking the dpHb–NAc projection while leaving the SCN undisturbed was sufficient to render mice insensitive to LAN (Fig. 4), further validating the notion that LAN affects behavior without perturbation of the circadian system. Additionally, we monitored the sleep/wake architecture of the mice during and after LAN exposure in both WT mice and mice with Tet-Tox-mediated permanent blockage of the dpHb–NAc projection (Extended Data Fig. 8a,b). Indeed, in the presence of a 2-h nighttime light pulse, both groups of mice exhibited decreased wakefulness and increased sleep as expected, which recovered immediately after lights-off (Extended Data Fig. 8c,d), and both groups of animals resumed normal sleep/wake architecture immediately after the termination of 3 week of LAN exposure (Extended Data Fig. 8e,f). Interestingly, animals with permanent blockage of the dpHb–NAc projection (Tet-Tox group, Extended Data Fig. 8d,f) experienced similar sleep disruptions to control animals, yet the Tet-Tox group did not develop depressive-like behaviors after 3-week LAN exposure (Extended Data Fig. 8g,h). These observations suggest that although LAN is accompanied by sleep disruption during the light pulse, such a disturbance does not play a causal role in the negative mood induced by LAN.

Using trans-synaptic tracing tools, we found the ipRGC-innervated pHb continued to project to brain areas that have been implicated in regulating depressive-like behaviors, namely NAc and mPFC. We further discovered that the pHb consists of two segregated populations of neurons. The innervations of pHb to the NAc predominantly originate from the neurons within the dorsal sector, whereas mPFC-projecting neurons reside in the vpHb, with only minimum overlap. More importantly, these two projections are also functionally distinct: only the dpHb–NAc projection is circadian gated (Fig. 3) and mediates the LAN-induced depressive-like behaviors (Fig. 4).

We speculate that the circadian modification of NAc-projecting dpHb neurons could occur either through direct synaptic inputs from circadian centers in the brain (SCN, IGL, and so on, Extended Data Fig. 5b) or via the local, endogenous circadian rhythm. Such circadian influence may result in periodic up/downregulation of the expression, altered localization or modification of certain cellular machinery, including voltage-dependent ion channels that are critical for determining neuronal excitability<sup>29,30</sup>. Since many neurological functions of mammals exhibit day/night fluctuations<sup>31,32</sup>, such a circadian gating mechanism may be shared by multiple physiological processes as a common strategy to coordinate circadian rhythm and neural activities.

A previous investigation in which CTB was delivered into the pHb showed that the pHb projected to multiple downstream sites, among which mPFC received the most innervation<sup>16</sup>. Interestingly, when we employed a more specific trans-synaptic anterograde tracing approach that selectively labeled the downstream projections of ipRGC-recipient pHb neurons, we found the NAc to be the most prominent target instead (Fig. 2). This apparent discrepancy likely arises from retinal-input-specific labeling versus global labeling of the pHb. Consistently, our photometric recordings of NAc- and mPFC-projecting pHb neurons also suggests that NAc-projecting pHb neurons are more readily responsive to light

stimulations under circadian modulations, supporting the notion that pHb–NAc projections play a prominent role in conveying retinal-specific signals.

Careful considerations should be given to the limitations of rodent models in light-related studies, particularly when applying findings from the present study to a human context. First of all, the rodent model used in our current study, the C57BL/6 mouse, is generally regarded as a melatonin-deficient model without detectable melatonin rhythms<sup>33,34</sup>, whereas humans have the light-sensitive melatonin secretion<sup>11</sup>. Whether and how melatonin fluctuations contribute to negative mood associated with nighttime light exposure in humans remains unclear. Further, light is an aversive signal to rodents, thereby possessing additional emotional valence in studies such as the present one. To precisely understand how light at night impacts human mood, future investigations should establish whether the pathway and mechanism identified here also exist in humans. Last but not least, there are on-going controversies regarding the accurate interpretation of rodent assays for ‘depression’ or ‘depressive’ phenotypes. For instance, the FST has been argued to be a measure of stress-coping but not necessarily depression-like behaviors<sup>35–37</sup>. In light of this, we only interpreted the results of FST in combination with SPT for indication of depressive-like states.

In summary, our study has elucidated a circadian-gated ipRGC→dpHb→NAc pathway that mediates the depressive-like behaviors induced by chronic exposure to light at night. Conceivably, this circuit might prompt animals to shy from unnecessary light exposure during the subjective night (as indicated by our RTPA experiments in Fig. 6), which might help the animal to avoid predators or to prevent disturbing their biological rhythms, especially during light transition periods such as dusk or dawn. However, unlike any other time in our evolutionary history, exposure to LAN is increasingly inevitable in the postindustrial era. Consequently, this pathway, which has been adapted to serve protective purposes, might be ‘hijacked’ to mediate LAN-induced negative mood in humans.

### Online content

Any methods, additional references, Nature Research reporting summaries, source data, extended data, supplementary information, acknowledgements, peer review information; details of author contributions and competing interests; and statements of data and code availability are available at <https://doi.org/10.1038/s41593-020-0640-8>.

Received: 20 February 2019; Accepted: 10 April 2020;

Published online: 1 June 2020

### References

- LeGates, T. A., Fernandez, D. C. & Hattar, S. Light as a central modulator of circadian rhythms, sleep and affect. *Nat. Rev. Neurosci.* **15**, 443–454 (2014).
- Vandewalle, G., Maquet, P. & Dijk, D. J. Light as a modulator of cognitive brain function. *Trends Cogn. Sci.* **13**, 429–438 (2009).
- Bais, B. et al. Bright light therapy in pregnant women with major depressive disorder: study protocol for a randomized, double-blind, controlled clinical trial. *BMC Psychiatry* **16**, 381 (2016).
- Golden, R. N. et al. The efficacy of light therapy in the treatment of mood disorders: a review and meta-analysis of the evidence. *Am. J. Psychiatry* **162**, 656–662 (2005).
- Lam, R. W. et al. Efficacy of bright light treatment, fluoxetine, and the combination in patients with nonseasonal major depressive disorder: a randomized clinical trial. *JAMA Psychiatry* **73**, 56–63 (2016).
- Bedrosian, T. A. & Nelson, R. J. Influence of the modern light environment on mood. *Mol. Psychiatry* **18**, 751–757 (2013).
- Zielinska-Dabkowska, K. M. Make lighting healthier. *Nature* **553**, 274–276 (2018).
- Scott, A. J., Monk, T. H. & Brink, L. L. Shiftwork as a risk factor for depression: a pilot study. *Int J. Occup. Environ. Health* **3**, S2–S9 (1997).
- Obayashi, K., Saeki, K., Iwamoto, J., Ikada, Y. & Kurumatani, N. Exposure to light at night and risk of depression in the elderly. *J. Affect Disord.* **151**, 331–336 (2013).
- Min, J. Y. & Min, K. B. Outdoor light at night and the prevalence of depressive symptoms and suicidal behaviors: a cross-sectional study in a nationally representative sample of Korean adults. *J. Affect Disord.* **227**, 199–205 (2018).
- Brzezinski, A. Melatonin in humans. *N. Engl. J. Med.* **336**, 186–195 (1997).
- Fonken, L. K., Aubrecht, T. G., Melendez-Fernandez, O. H., Weil, Z. M. & Nelson, R. J. Dim light at night disrupts molecular circadian rhythms and increases body weight. *J. Biol. Rhythms* **28**, 262–271 (2013).
- Stevens, R. G. Working against our endogenous circadian clock: breast cancer and electric lighting in the modern world. *Mutat. Res* **680**, 106–108 (2009).
- Lyall, L. M. et al. Association of disrupted circadian rhythmicity with mood disorders, subjective wellbeing, and cognitive function: a cross-sectional study of 91 105 participants from the UK Biobank. *Lancet Psychiatry* **5**, 507–514 (2018).
- Vandewalle, G. et al. Spectral quality of light modulates emotional brain responses in humans. *Proc. Natl Acad. Sci. USA* **107**, 19549–19554 (2010).
- Fernandez, D. C. Light affects mood and learning through distinct retina-brain pathways. *Cell* **175**, 71–84.e18 (2018).
- Berson, D. M., Dunn, F. A. & Takao, M. Phototransduction by retinal ganglion cells that set the circadian clock. *Science* **295**, 1070–1073 (2002).
- Do, M. T. & Yau, K. W. Intrinsically photosensitive retinal ganglion cells. *Physiol. Rev.* **90**, 1547–1581 (2010).
- Fu, Y. et al. Intrinsically photosensitive retinal ganglion cells detect light with a vitamin A-based photopigment, melanopsin. *Proc. Natl Acad. Sci. USA* **102**, 10339–10344 (2005).
- Hattar, S. et al. Central projections of melanopsin-expressing retinal ganglion cells in the mouse. *J. Comp. Neurol.* **497**, 326–349 (2006).
- Dunlap, J. C. Molecular bases for circadian clocks. *Cell* **96**, 271–290 (1999).
- Lowrey, P. L. & Takahashi, J. S. Genetics of the mammalian circadian system: photic entrainment, circadian pacemaker mechanisms, and posttranslational regulation. *Annu Rev. Genet.* **34**, 533–562 (2000).
- Buhr, E. D. & Van Gelder, R. N. Local photic entrainment of the retinal circadian oscillator in the absence of rods, cones, and melanopsin. *Proc. Natl Acad. Sci. USA* **111**, 8625–8630 (2014).
- Zhang, J., Wang, H., Wu, S., Liu, Q. & Wang, N. Regulation of reentrainment function is dependent on a certain minimal number of intact functional ipRGCs in rd mice. *J. Ophthalmol.* **2017**, 6804853 (2017).
- Zingg, B. et al. AAV-mediated anterograde transsynaptic tagging: mapping corticocolligular input-defined neural pathways for defense behaviors. *Neuron* **93**, 33–47 (2017).
- Hu, H. Reward and aversion. *Annu Rev. Neurosci.* **39**, 297–324 (2016).
- Russo, S. J. & Nestler, E. J. The brain reward circuitry in mood disorders. *Nat. Rev. Neurosci.* **14**, 609–625 (2013).
- Hannibal, J. Neurotransmitters of the retino-hypothalamic tract. *Cell Tissue Res* **309**, 73–88 (2002).
- Whitt, J. P., Montgomery, J. R. & Meredith, A. L. BK channel inactivation gates daytime excitability in the circadian clock. *Nat. Commun.* **7**, 10837 (2016).
- Flourakis, M. et al. A conserved bicycle model for circadian clock control of membrane excitability. *Cell* **162**, 836–848 (2015).
- Rothen, N. & Meier, B. Time of day affects implicit memory for unattended stimuli. *Conscious Cogn.* **46**, 1–6 (2016).
- Russo, K. A. et al. Circadian control of the female reproductive axis through gated responsiveness of the RFRP-3 system to VIP signaling. *Endocrinology* **156**, 2608–2618 (2015).
- Goto, M., Oshima, I., Tomita, T. & Ebihara, S. Melatonin content of the pineal gland in different mouse strains. *J. Pineal. Res.* **7**, 195–204 (1989).
- Roseboom, P. H. et al. Natural melatonin ‘knockdown’ in C57BL/6J mice: rare mechanism truncates serotonin N-acetyltransferase. *Brain Res Mol. Brain Res* **63**, 189–197 (1998).
- Commons, K. G., Cholanians, A. B., Babb, J. A. & Ehlinger, D. G. The rodent forced swim test measures stress-coping strategy, not depression-like behavior. *ACS Chem. Neurosci.* **8**, 955–960 (2017).
- Reardon, S. Depression researchers rethink popular mouse swim tests. *Nature* **571**, 456–457 (2019).
- Molendijk, M. L. & de Kloet, E. R. Immobility in the forced swim test is adaptive and does not reflect depression. *Psychoneuroendocrinology* **62**, 389–391 (2015).

**Publisher's note** Springer Nature remains neutral with regard to jurisdictional claims in published maps and institutional affiliations.

© The Author(s), under exclusive licence to Springer Nature America, Inc. 2020

## Methods

**Animals.** All animal procedures were approved by the Institutional Animal Care and Use Committees at the University of Science and Technology of China (USTC) and the Chinese Academy of Sciences (CAS). Adult mice (2–4 months old, male and female C57BL/6 or transgenic mice as specified) were housed at a constant temperature with ad libitum access to standard rodent diet under a 8:00 to 20:00 12 h:12 h light/dark cycle (~200 lux white ambient illumination) except for during LAN exposure (~400 lux blue illumination between 21:00 and 23:00). Locomotor activities were assessed using a customized wheel-running system. All WT mice used in this study were obtained from the Model Animal Research Center of Nanjing University. Mice with a point mutation of the *Pde6b* gene (gene ID: 18587) that results in rod degeneration (*rd1/rd1*) and expressing cone-specific diphtheria toxin A (cone-DTA; *cDTA*) that leads to cone ablation on the background of C57BL/6 were also used as controls. *rd1/rd1;cDTA;Opn4<sup>-/-</sup>* and *Opn4-cre* mice were generous gifts from K.-W. Yau at Johns Hopkins University. *Rosa-DTA* mice were provided by X. Yu at Shandong University. The ipRGC ablation in *Opn4-cre;Rosa-DTA* mice was nearly complete beyond 3 months as verified by routine melanopsin immunostaining of the retina, with less than 30 positive cells in a whole flat-mount retina. Thus all DTA mice used in the current study were over three months old.

**Drugs.** Unless otherwise stated, all drugs were purchased from Sigma-Aldrich. Tetrodotoxin (TTX) was obtained from Dalian Refine Biochemical Items Co., Ltd, and sucrose was purchased from Sangon Biotech.

**Anterograde and retrograde tracers and viruses.** The following fluorescent tracing dyes or viral tools were employed in the current study: Herpes simplex virus (HSV-129, generous gift from M.-H. Luo) was used for anterograde trans-synaptic tracing. Alexafluor 555-conjugated cholera toxin subunit B (CTB-555, Thermo Fisher) and CTB-488 (BrainVTA) were used for anterograde or retrograde tracing. AAV2/2-EF1 $\alpha$ -DIO-ChR2-eYFP was used in intraocular injections to Cre-dependently express ChR2 and yellow fluorescence. AAV1-Cre (scAAV2/1-hSyn-Cre-pA) was used to express Cre recombinase in postsynaptic neurons to achieve input-specific labeling. AAV2/9-EF1 $\alpha$ -DIO-ChR2-eYFP was used to Cre-dependently express ChR2 in central neurons, while AAV2/9-CAG-FLEX-GFP was used to Cre-dependently express GFP in central neurons. RetroAAV2/2-Syn-Cre was used to retrogradely express Cre recombinase in the neurons projecting to the injection site through terminal absorption. AAV2/1-CAG-DIO-hm3Dq-mCherry and AAV2/9-hSyn-DIO-hm4Di-mCherry were used to Cre-dependently express the excitatory and the inhibitory DREADD in central neurons, respectively. AAV2/8-EF1 $\alpha$ -DIO-mCherry was used for Cre-dependent expression of mCherry as controls. AAV2/1-DIO-eGFP-Tet-Tox was used to Cre-dependently express the light chain of tetanus toxin (Tet-Tox) in central neurons. AAV2/5-hEF1 $\alpha$ -DIO-RVG was used to Cre-dependently express G protein that reinstated the trans-synaptic capability of rabies virus (RV) and AAV2/5-hEF1 $\alpha$ -DIO-H2B-eGFP-T2A-TVA was employed to direct the infection of modified RV. RV-EnvA- $\Delta$ G-dsRed was purchased from BrainVTA and used in conjunction with the aforementioned helper viruses for retrograde trans-synaptic tracing. AAV2/1-hSyn-FLEX-GCaMP6s was used in optic photometry recordings.

AAV2/1-DIO-eGFP-Tet-Tox and AAV2/1-hSyn-DIO-hm3Dq-mCherry were prepared in the Xue laboratory. AAV2/9-CAG-FLEX-GFP was obtained from OBiO Technology (Shanghai) Corp., Ltd. All other AAV tools were prepared by Shanghai Taitool Bioscience.

**Intraocular injection.** The dilating eye drop (1% w/v Atropin and 5% w/v phenylephrine hydrochloride) was applied to dilate the pupils. After approximately 5 min or until the pupils were fully dilated, mice were anesthetized with pentobarbital (i.p. 100 mg kg<sup>-1</sup>), and eye gel (5% sodium carboxymethyl cellulose) was used to prevent eyes from drying. The eyeball was then penetrated through the pupil with the tip of a 26 gauge needle under the stereoscope to release the ocular pressure, immediately followed by the injection of 1.5  $\mu$ l of virus or tracing dye into the space between the lens and the retina using a Hamilton syringe (Model 65 RN SYR with 33 gauge customized needle). Following surgery, mice were allowed to recover from anesthesia on a heating mat before being returned to their home cages, and the ones with noticeable bleeding or damage to the retina were excluded from further experiments.

**Stereotaxic injection and optical fiber implantation.** Adult mouse was anesthetized with pentobarbital (i.p. 100 mg kg<sup>-1</sup>) and mounted on a stereotaxic apparatus (Shenzhen RWD Life Science). Erythromycin ointment (Guangdong Hengjian Pharmaceutical Co., Ltd) was applied to keep the corneal moist. The scalp was shaved and cleansed, and then a linear incision on the skin was made to expose the skull, which was subsequently cleaned with a cotton swab dipped in PBS. The skull above the target area was drilled open and 150 nl of virus or 60 nl of dye was delivered into the brain at the rate of 30 nl min<sup>-1</sup>. The coordinates, defined as dorsal–ventral (DV) from the brain surface, anterior–posterior (AP) from bregma and medial–lateral (ML) from the midline, were as follows: NAc (AP, +1.80 mm from bregma; ML,  $\pm$ 0.9 mm; DV, –3.73 mm); mPFC (AP, +1.90 mm

from bregma; ML,  $\pm$ 0.5 mm; DV, –1.5 mm); pHb (AP, –1.60 mm from bregma; ML,  $\pm$ 0.65 mm; DV, –2.55 mm). After completion of the injection including a 10-min delay, the injection pipette was slowly withdrawn and the scalp was sutured back. For excitotoxic lesion, 50 nl of solution of NMDA (22 mM) was injected at 20 nl min<sup>-1</sup> with an additional 15-min delay to prevent leakage and to ensure localized lesion. An equal volume of PBS was injected in the sham-operated control animal. The effective lesion was verified post hoc through glial fibrillary acidic protein (GFAP) staining. For the data presented in Fig. 2, one animal was removed from the NMDA lesion group due to incomplete lesion revealed by GFAP staining. In the case of optogenetic experiments, bilateral optical fiber implantation was conducted with a 15° angle (pHb: AP, –1.60 mm from bregma; ML,  $\pm$ 1.45 mm; DV, –2.6 mm) immediately after virus injection. The optical fiber (200  $\mu$ m outer diameter (O.D.), AniLab) was fitted into a ceramic fiber holder that was fixed in place using 3M Vetbond Tissue Adhesive and a denture base material mixed with black dye to avoid light leaking from the junction. Animals were allowed to recover for at least 1 week before behavioral experiments.

**Electrophysiology.** Animals were sacrificed under deep anesthesia, and the brain was removed and placed for 1 min in cold (0–4°C) cutting solution containing (in mM): 60 NaCl, 1.25 KCl, 25 NaHCO<sub>3</sub>, 1.25 KH<sub>2</sub>PO<sub>4</sub>, 25 D-glucose, 0.1 CaCl<sub>2</sub>, 3 MgCl<sub>2</sub> and 120 sucrose, adjusted to 300–310 mOsm. For relatively older animals, an N-methyl-D-glucamine (NMDG)-based cutting solution was used that contained (in mM): 92 NMDG, 1.2 KCl, 1.2 KH<sub>2</sub>PO<sub>4</sub>, 30 NaHCO<sub>3</sub>, 25 D-glucose, 3 Na-pyruvate, 5 L-ascorbic acid, 2 thiourea, 10 MgSO<sub>4</sub>, 20 HEPES, 0.5 CaCl<sub>2</sub>, adjusted to pH = 7.3 using HCl. Coronal slices (300  $\mu$ m thick) were made on a vibrating microtome (Lieva VT-1200S), and then allowed to recover for 40 min at 37°C in artificial cerebral spinal fluid (aCSF) containing (in mM): 125 NaCl, 1.25 KCl, 1.23 KH<sub>2</sub>PO<sub>4</sub>, 25 NaHCO<sub>3</sub>, 2 CaCl<sub>2</sub>, 1 MgCl<sub>2</sub> and 25 D-glucose, bubbled with 95% O<sub>2</sub>/5% CO<sub>2</sub>, adjusted to pH = 7.3, 300–310 mOsm.

After recovery, brain slices were transferred to the recording chamber perfused with oxygenized aCSF at room temperature. Recording pipettes were pulled from borosilicate glass capillaries (O.D. 1.5 mm, inner diameter (I.D.) 0.86 mm, Sutter Instruments) on a horizontal puller (P1000, Sutter Instruments) to a tip resistance of 4–6 M $\Omega$  when filled with internal recording solution containing (in mM): 10 KCl, 125 potassium-gluconate, 0.1 EGTA and 10 HEPES, supplemented with 5 ATP-Mg and 0.5 GTP-Na, adjusted to pH = 7.3, 295–300 mOsm. Cells were visualized under differential interference contrast (DIC) microscopy and identified via fluorescence if applicable. Once a steady whole-cell recording configuration was achieved, the neuron was challenged with either optogenetic stimulation of 470-nm light pulses generated by a commercial light emitting diode (LED) or current steps from –50 pA to 90 pA in 10-pA increment. Cells that appeared unhealthy (input resistance lower than 150 M $\Omega$  or resting membrane potential positive than –40 mV) or without adequate access (access resistance higher than 30 M $\Omega$  or initial action potential not reaching +20 mV) were excluded from data analysis. Voltage-clamp and current-clamp recordings were made with a Multiclamp 700B amplifier and a Digidata 1440A digitizer (Axon Instruments). Data was acquired with Axon pClamp software (v.9.2, Molecular Devices), low-pass filtered at 1,000 Hz and sampled at 20 kHz.

To assess the nature of the dpHb–NAC neurotransmission, an internal solution was used with elevated chloride concentration containing (in mM): 135 KCl, 0.1 EGTA and 10 HEPES, supplemented with 5 ATP-Mg and 0.5 GTP-Na, adjusted to pH = 7.3. This high-Cl<sup>-</sup> internal solution yielded a Cl<sup>-</sup> reversal potential of ~0 mV. Therefore, when the cell was held at –70 mV, both excitatory and inhibitory postsynaptic currents (EPSCs and IPSCs) were downward. Upon successful establishment of a whole-cell configuration, NAC neurons were first checked for optogenetically evoked PSCs. The ones without detectable PSCs or those receiving apparent polysynaptic inputs (judged by the high jitter and frequent failures) were discarded. Only neurons receiving inputs with stable monosynaptic components were pursued, and the monosynaptic inputs were isolated with bath perfusion of 100 nM TTX + 40  $\mu$ M 4-aminopyridine (4AP) (Sigma-Aldrich; 275875) for at least 20 min. The isolated monosynaptic PSCs were then challenged sequentially with 40  $\mu$ M PTX (Sigma-Aldrich; P1675) and 20  $\mu$ M CNQX (Sigma-Aldrich; C239) to determine the nature of the neurotransmission.

For experiments in Fig. 3, dark/day and light/night conditions were applied. Under dark/day conditions, mice were maintained under regular 8:00 to 20:00 photoperiods and kept in the dark after 8:00 on the day of the experiment for ~1 h before being euthanized in the dark, followed by electrophysiological recordings. Likewise, animals in the light/night group were kept under regular photoperiods and only remained in an illuminated environment after 20:00 for ~1 h on the day of the experiment, followed by preparation of the brain slices and electrophysiological recordings under normal light conditions.

**Randomization and blinding.** For behavioral experiments, electrophysiological recordings, photometry recordings and EEG recordings, littermates were randomly assigned to various treatment groups. In any specific experiment, animals were examined in a semi-randomized order, with alternate control and experimental animals. The experimenters who collected the data were not blind to the group assignment of the object, because they needed to record the identifier of the sample or animal. However, data were analyzed either by automated software using

consistent parameters or by investigators who were blind to the experimental conditions.

**FST.** FST was performed as previously established, normally during the time period 8:00 to 11:00 unless otherwise specified. Briefly, animals were individually placed in a glass cylinder filled with warm water (25 °C) to ~15 cm from the bottom under normal illumination. The behavior of the animal was recorded by the camera from the side for off-line analysis. Duration of immobility was counted by the same observer throughout the study as the time when the mice remained floating without any noticeable voluntary movement of either the head or any of the four limbs. Only the last 4 min of each trial were analyzed, averaged, and presented as  $s \text{ min}^{-1}$ . For chemogenetic manipulations, each mouse was tested on two consecutive days, and on each day received either a single injection of CNO (1 mg kg<sup>-1</sup>) or an equal volume of PBS. FST was conducted 30 min after the injection on both days. The order of treatments (CNO on the first day and PBS on the second day or vice versa) for each mouse was evenly and strategically assigned to ensure that any systemic variation was well controlled for. One animal in Fig. 4c and one in Fig. 6g were excluded from further experiments due to extreme basal levels (0 s immobility time at baseline), which were well below the average immobility time of naïve/WT mice in our experience and might indicate an abnormal locomotor status or anxiety-like emotional states. To prevent introducing variables that might interfere with the interpretation of behavioral results, no further assessments were performed on these animals.

**SPT.** Mice were single housed to acclimatize to two bottles of water for 24 h, then subjected to water deprivation for 24 h, followed by the 24-h testing period (starting from 14:00) during which the mice were provided with one bottle of 1% sucrose and one bottle of water. The position of the two bottles was switched at 2 h and 6 h. Sucrose preference was calculated as the proportion of 1% sucrose in the total liquid consumed (water and sucrose). For optogenetic manipulations, sucrose preference was monitored from 20:00 to 22:00. One hour of optostimulation was applied either during the first or the second hour, with the nonstimulated hour as the baseline period. The positions of the two bottles were switched every 30 min. To minimize the impact of the higher drinking drive during the first hour, the sequence of stimulation (stimulation first or baseline first) was randomized and strategized to ensure an unbiased and comparable assignment between the experimental group and the control group. For chemogenetic experiments, sucrose preference was monitored from 20:00 to 23:00, with a single injection of either CNO (1 mg kg<sup>-1</sup>) or PBS 30 min before the test. Bottles were switched at 30 min, 1 h and 2 h. After the test, animals were allowed to recover for a day with two bottles of water and then subjected to a second round of SPT. Mice that received CNO during the first test were given PBS during the second test and vice versa. The order of injections was evenly and strategically assigned to experimental and control groups.

**RTPA.** The RTPA was performed during the period 8:00 to 11:00 as previously established<sup>38</sup>. In brief, the mouse was placed in the middle of an arena (72 × 30 × 30 cm<sup>3</sup>) consisting of two chambers connected by a 'neck' structure. The animal was allowed to freely explore both chambers for 20 min. The time spent in each chamber was counted by an observer to determine the baseline place preference, and the preferred chamber was designated as the 'stimulation' side during the subsequent 20 min testing period. During test, optostimulation was delivered whenever the mouse entered the 'stimulation' chamber and lasted as long as the mouse remained inside. The behavior was recorded from above by a video camera, and time spent in each chamber was counted off-line by the same observer. Videos from the baseline as well as the testing period were also analyzed using Ethovision software (v.XT 8.5) to verify the counting of the observer regarding the initial preference. Values generated with Ethovision were used to calculate the avoidance score as (Time in stimulated side - Time in nonstimulated side)<sub>test</sub> - (Time in stimulated side - Time in nonstimulated side)<sub>baseline</sub>.

**TST.** Mice were allowed to acclimatize to the handling of the experimenter and the experimental space in their home cages for at least 3 d before TST, so as to minimize the stress of the animals. On the day of the experiment, during the period 8:00 to 11:00 unless otherwise specified, a tape loop was attached to the tail of the mouse, and the optic fiber was plugged in position in the case of the optogenetic experiments. Then the animal was returned to its home cage for 30 min. During TST, the mouse was suspended by the tail loop at least 15 cm from the horizontal bar (to avoid climbing). The behavior of the animal was recorded by a side camera and the duration of immobility was counted off-line by the same experimenter. The first 2 min were excluded due to high stress, and the immobility was averaged from 3 min of either baseline or during optostimulation and presented as  $s \text{ min}^{-1}$ .

**Optogenetics.** Before optogenetic experiments, mice were routinely handled by the experimenter for at least three consecutive days. On the day of the experiment, the optical fiber was plugged into the ferrule and then the mouse was returned to its home cage for 15 min. During optostimulation, a 473-nm blue laser was delivered at 10 Hz and 10% duty cycle with 2.8–4.7 mW for soma stimulation and 6.6–9.1 mW for terminal activation. After the termination of the experiments,

brain samples were harvested, sectioned and imaged, to verify the adequate viral expression and correct placement of the optical fiber.

**Chronic chemogenetic activation.** For the chronic model presented in Fig. 6i–k, mice that selectively expressed hM3D in NAc-projecting dpHb neurons received daily CNO (regular H<sub>2</sub>O for the control group) in drinking water during the period 20:00 to 23:00 for three consecutive weeks. The mice were supplied with regular drinking water from 23:00 to 8:00 the next morning, and then water deprived for 12 h until the next round of CNO delivery. The affective behaviors of the animals were examined before and after 3 weeks of chronic CNO administration.

**Immunohistochemistry.** Mice anesthetized with pentobarbital (100 mg kg<sup>-1</sup>) were perfused intracardially with PBS, followed by 4% paraformaldehyde (PFA, w/v in PBS). Then brain was removed, postfixed in 4% PFA at 4 °C for 24 h, and then dehydrated in 30% sucrose solution. Coronal sections were made on a Cryostat microtome (Leica CM3050S) at 40 μm thickness, blocked with blocking solution (PBS containing 5% BSA, 5% goat serum and 0.5% Triton X-100 as appropriate) for 1 h at room temperature and then incubated with the appropriate primary antibody (antibodies) for 48 h at 4 °C. The primary antibodies used in the present study are as follows: rabbit anti-GABA (Sigma-Aldrich A2052; 1:500; research resource identifier (RRID) AB\_477652; lot no. 018M4808V); rabbit anti-glutamate (Sigma-Aldrich G6642; 1:500; RRID AB\_259946; lot no. 108M4860V); rabbit anti-GFAP (Sangon Biotech D120691; 1:200); rabbit anti-c-fos (Synaptic Systems 226003; 1:5,000; RRID AB\_2231974; lot no. 7-78); rabbit anti-melanopsin (Advanced Targeting System, AB-N38, 1:10,000; RRID AB\_1266797; lot no. 112-16); rabbit anti-per1 (Abcam ab136451, 1:500; lot no. GR3216520-2). After the incubation with primary antibody, sections were washed with PBS (3 × 5 min) and then incubated with secondary antibodies for 1 h at room temperature. Secondary antibodies used in the present study are as follows: Alexa Fluor 568 (Thermo Fisher A-11036, 1:500; RRID AB\_10563566; lot no. 2155282) and Alexa Fluor 488 (Thermo Fisher A-11034, 1:500; RRID AB\_2576217; lot no. 2069632). For Per1 immunostaining presented in Fig. 1f, mice from both groups were dark-adapted for 24 h and kept in the dark until sacrificed at ZT 1, 5, 9, 13, 17 or 21.

For retinal immunostaining, the mice were euthanized and the eyes were removed and fixed in 4% (w/v) paraformaldehyde for 2 h at room temperature. After the fixation, the cornea was cut off and the vitreous was cleaned up. The retina was then isolated and subjected to routine immunohistochemistry (IHC) procedure. Finally, the sections were examined and imaged under a Leica two-photon microscope (SP8, Leica).

For further details regarding the validation of antibodies, please refer to the Nature Science Reporting Summary attached to this article.

**Fiber photometry.** Animals received administration of retroAAV2/2-Syn-Cre into NAc or mPFC and AAV2/1-hSyn-FLEX-GCaMP6s into pHb. Immediately following virus injection, an optic fiber (200 μm O.D., numerical aperture = 0.37; 3 mm length; AniLab Software & Instrument Co., Ltd) was placed in a ceramic holder, implanted into pHb and fixed in position using the dental acrylic.

Photometric recordings were conducted using the fiber photometry recording system (THINKERTECH) 3 weeks after the surgical procedures to ensure adequate animal recovery and virus expression. A 473-nm LED light beam (50 μW) (Cree XPE LED) was reflected by a dichroic mirror (MD498; Thorlabs) and a ×20 objective lens (numerical aperture = 0.4; Olympus). The fluorescence from GCaMP was bandpass filtered (MF525-39, Thorlabs) and collected by a photomultiplier tube (H10721-210, Hamamatsu), which was further low-pass filtered (40 Hz cut-off; THINKERTECH) and digitalized at 100 Hz. To record the activity of NAc-projecting dpHb neurons, the optic fiber was attached to freely moving animals that were housed in their home cages and then placed in a light-proof enclosure to habituate and dark adapt for 30 min. Each trial consisted of 120 s baseline and 10 runs of 100 s (20 s light then 80 s dark). Ambient blue (473 nm) light at 0.66 mW cm<sup>-2</sup> (1.56 × 15 photons cm<sup>-2</sup> s<sup>-1</sup>) was applied as the stimulation. Data for the 'day' group were collected during the period 9:00 to 12:00, and data for the 'night' group were collected during the period 21:00 to 24:00. All photometric data were analyzed using a customized script written in MATLAB software (v.2017b) with autofluorescence subtraction. After the termination of the experiments, brain samples were harvested, sectioned and imaged, to verify the adequate viral expression and correct placement of the optical fiber. Six recording sites from six animals (NAc) and four recording sites from three animals (mPFC) were excluded from final analysis due to unsatisfactory expression of viruses (fewer than ten cells) or incorrect placement of the optical fiber (located outside the pHb area and the vicinity above the pHb).

**Electrode implants.** Three weeks after the stereotaxical injection of virus, the mice were anesthetized by pentobarbital (i.p. 100 mg kg<sup>-1</sup>), and then implanted with electrodes for electroencephalogram (EEG) and electromyogram (EMG) recordings<sup>39</sup>. In brief, two EEG screw electrodes were implanted into the skull and two flexible EMG wire electrodes were placed into the nuchal muscles. The free ends of the leads were soldered into a head socket, which was then attached to the skull using dental cement. Postoperatively, animals were housed in their home cages for recovery and LAN treatments.

**EEG/EMG recording and sleep/wake scoring.** After postoperative recovery, each mouse was connected to an EEG/EMG recording cable in a soundproof recording chamber and habituated for 3 d before polygraphic recording. The EEG/EMG signals were amplified, filtered (EEG, 0.5–30 Hz; EMG, 20–200 Hz), digitized at a sampling rate of 128 Hz and recorded using Sleepsign software (v.2.0, Kissei Comtec). Sleep/wakefulness states were monitored for a period of 24 h beginning from lights on (8:00). We performed EEG and EMG recordings 2 or 3 d before, during and after LAN exposure. The EEG/EMG recording data were automatically scored off-line in 10 s epochs to sort wake, REM or slow-wave sleep, using Sleepsign. This was conducted according to previously established criteria<sup>40</sup>. As a final step, defined sleep/wake stages were examined visually, and corrected if necessary. Scoring was done before histological examination and therefore scorers were unaware of the extent of receptor expression. EEG data presented in Extended Data Fig. 8 were collected from three mice, and for each animal data were averaged from 2 to 3 d of consecutive recordings. Data from another two animals were excluded due to large and frequent noise in the recordings, which greatly hindered an accurate sleep/wake scoring.

**Statistics and reproducibility.** Data were presented as mean  $\pm$  s.d. with the exception of Figs. 3e,g,j and 5i,j,l,m and Extended Data Fig. 8c–f in which s.e.m. was used for the purpose of clarity. No statistical methods were used to predetermine sample sizes. Sample sizes were indicated in the figures and associated text, and are similar to those reported in previous studies<sup>41,42</sup>. The normality of the data distribution was confirmed by the D'Agostino–Pearson normality test and Shapiro–Wilk normality test. Statistical differences of normally distributed data were then determined using paired or unpaired two-tailed *t*-test, and one-way or two-way analysis of variance (ANOVA) followed by Sidak's, Bonferroni's or Tukey's multiple comparison tests as indicated in the figure captions. In general, *t*-tests were used to compare data before and after LAN exposure. ANOVA was used to determine the alterations in the intrinsic excitability of pHb neurons. Two-tailed unpaired *t*-tests were performed with Welch's correction to adjust for unequal variance. The two-sided Wilcoxon matched-pairs signed rank test was employed to analyze non-normally distributed data. *P* values less than 0.05 were considered significant. For further detail regarding the inclusion and exclusion criteria, data reproducibility and data analysis, please refer to the Nature Research Reporting Summary attached to this article.

**Reporting Summary.** Further information on research design is available in the Nature Research Reporting Summary linked to this article.

### Data availability

The data that support the findings of this study, besides what has been included in this manuscript (including the supplemental section), are available from the corresponding authors (T.X.) upon request.

### Code availability

The customized codes used to generate the results are available from the corresponding authors upon reasonable request.

### References

38. Yang, Y. et al. Ketamine blocks bursting in the lateral habenula to rapidly relieve depression. *Nature* **554**, 317–322 (2018).

39. Oishi, Y. et al. Slow-wave sleep is controlled by a subset of nucleus accumbens core neurons in mice. *Nat. Commun.* **8**, 734 (2017).  
 40. Xu, Q. et al. A mouse model mimicking human first night effect for the evaluation of hypnotics. *Pharm. Biochem. Behav.* **116**, 129–136 (2014).  
 41. Menard, C. et al. Social stress induces neurovascular pathology promoting depression. *Nat. Neurosci.* **20**, 1752–1760 (2017).  
 42. Huang, J. et al. A neuronal circuit for activating descending modulation of neuropathic pain. *Nat. Neurosci.* **22**, 1659–1668 (2019).

### Acknowledgements

The authors thank L.Q. Luo, X.K. Chen, Z.L. Qiu and X.H. Xu for their critical reading of the manuscript and their insightful advice. We also thank Y. Cai and X.Y. Zhou for their intellectual input and technical support. We thank members of the Neuroscience Pioneer Club for insightful discussions throughout the course of this study. This work was funded by the Strategic Priority Research Program of the Chinese Academy of Science (grant no. XDA16020603 to T.X.), the National Natural Science Foundation of China (grant nos. 81790644, 81925009 and 91432104 to T.X., 61890953 to J.B., 31601134 and 61727811 to H.Z., 91432104 to J.-T.C. and 81900855 to M.Z.), the Anhui Provincial Natural Science Foundation (grant no. 1708085QC57 to H.Z., 1808085MH289 to M.Z. and 1908085MC66 to J.-J.M.), the National Key Basic Research Program of China (grant no. 2016YFA0400900 to T.X.), the CAS priority research program (grant nos. XDPB10 and XDB02010000 to T.X.), the Innovative Program (grant no. ZT00102901 to H.Z.), the User with Excellence Program of Hefei Science Center CAS (grant no. 2019HSC-UE018 to T.X.), the Fundamental Research Funds for the Central Universities (grant no. WK2070000174 to T.X., M.Z. and Y.-Q. M.) and The Key Program in the Youth Elite Support Plan in Universities of Anhui Province (grant no. gxyqZD2018020 to Q.X.).

### Author contributions

T.X. conceived the idea. T.X., H.Z. and K.A. designed the study. K.A. performed all viral tracing, immunostaining and behavioral experiments with the help of Y.M., Y.-E.L. and J.-T.C. Y.-Q.M. and Y.-M.S. helped with tracing experiments. J.B. helped with setting up the actogram recording system. H.Z. and K.A. performed all electrophysiological recordings. J.-W.S. helped with in vivo photometry recordings and J.-J.M. analyzed photometry data. Q.X. performed the EEG recordings and analyzed the EEG data with the help of K.A. K.A. and H.Z. analyzed all other data and generated figures. T.X., H.Z. and K.A. interpreted the results with critical inputs from Y.-G.Y., M.Z. and Z.Z. H.Z., K.A. and T.X. wrote the manuscript.

### Competing interests

Authors declare no competing interests.

### Additional information

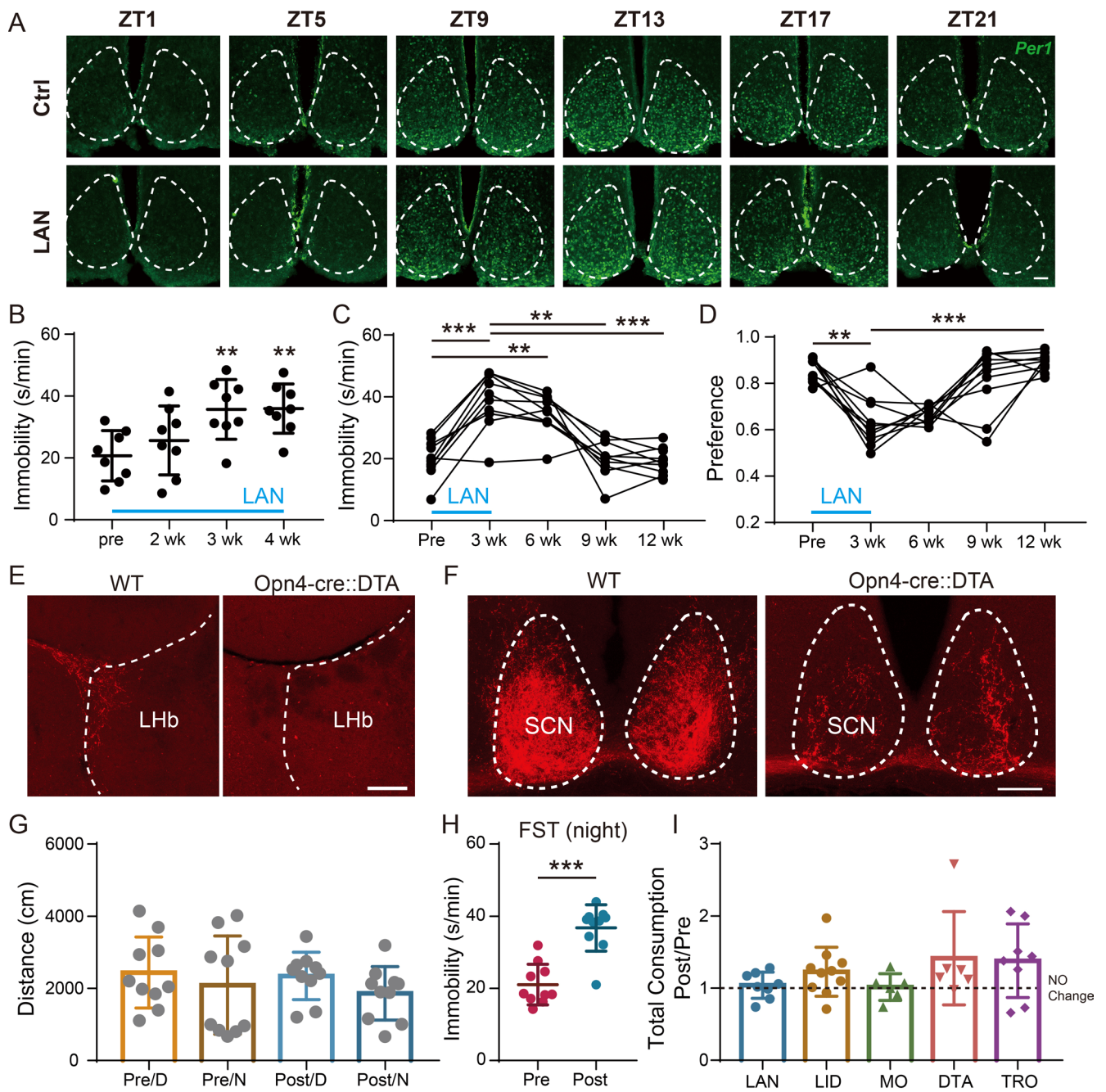
**Extended data** is available for this paper at <https://doi.org/10.1038/s41593-020-0640-8>.

**Supplementary information** is available for this paper at <https://doi.org/10.1038/s41593-020-0640-8>.

**Correspondence and requests for materials** should be addressed to H.Z. or T.X.

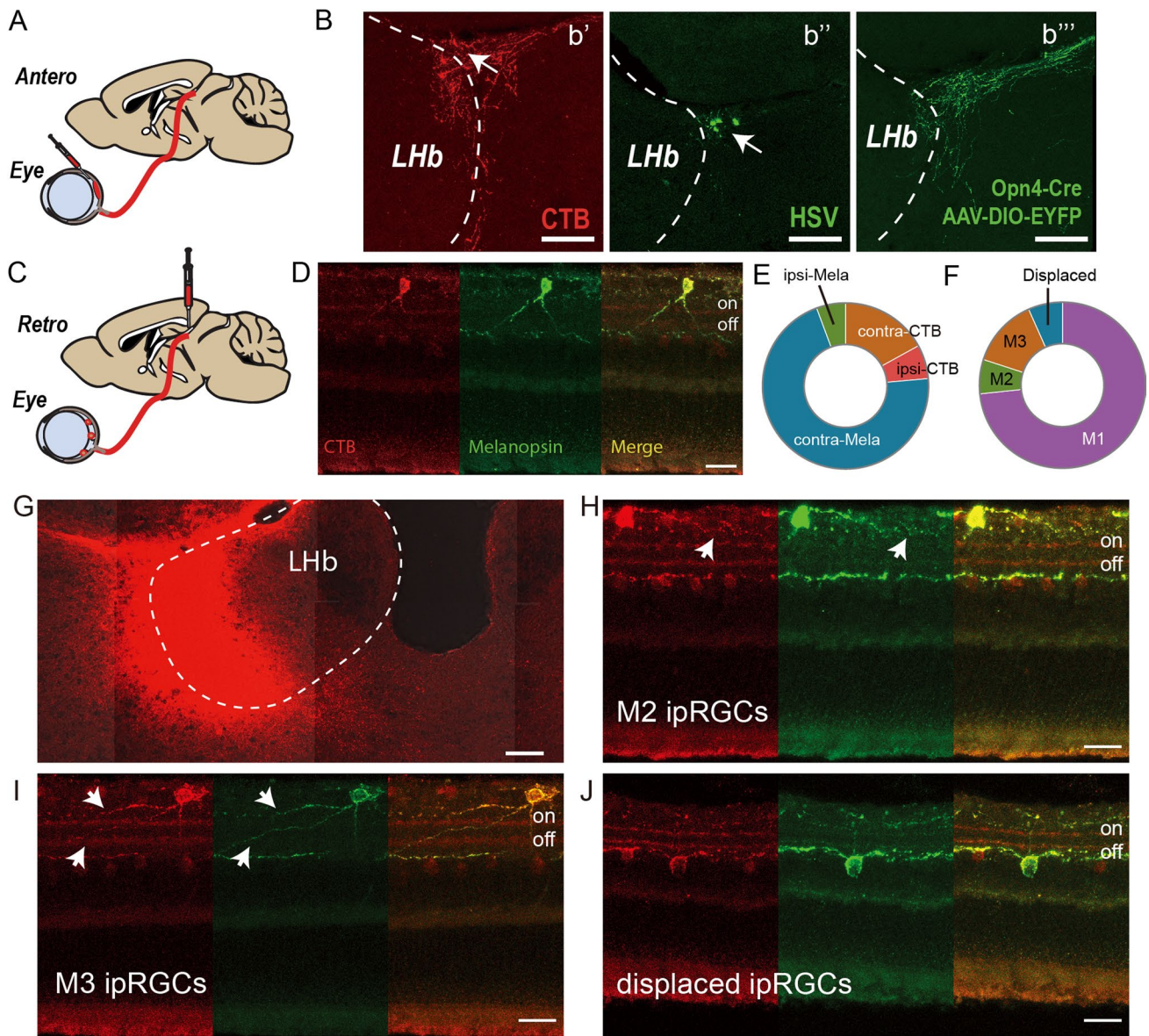
**Peer review information** *Nature Neuroscience* thanks Mario Penzo and the other, anonymous, reviewer(s) for their contribution to the peer review of this work.

**Reprints and permissions information** is available at [www.nature.com/reprints](http://www.nature.com/reprints).

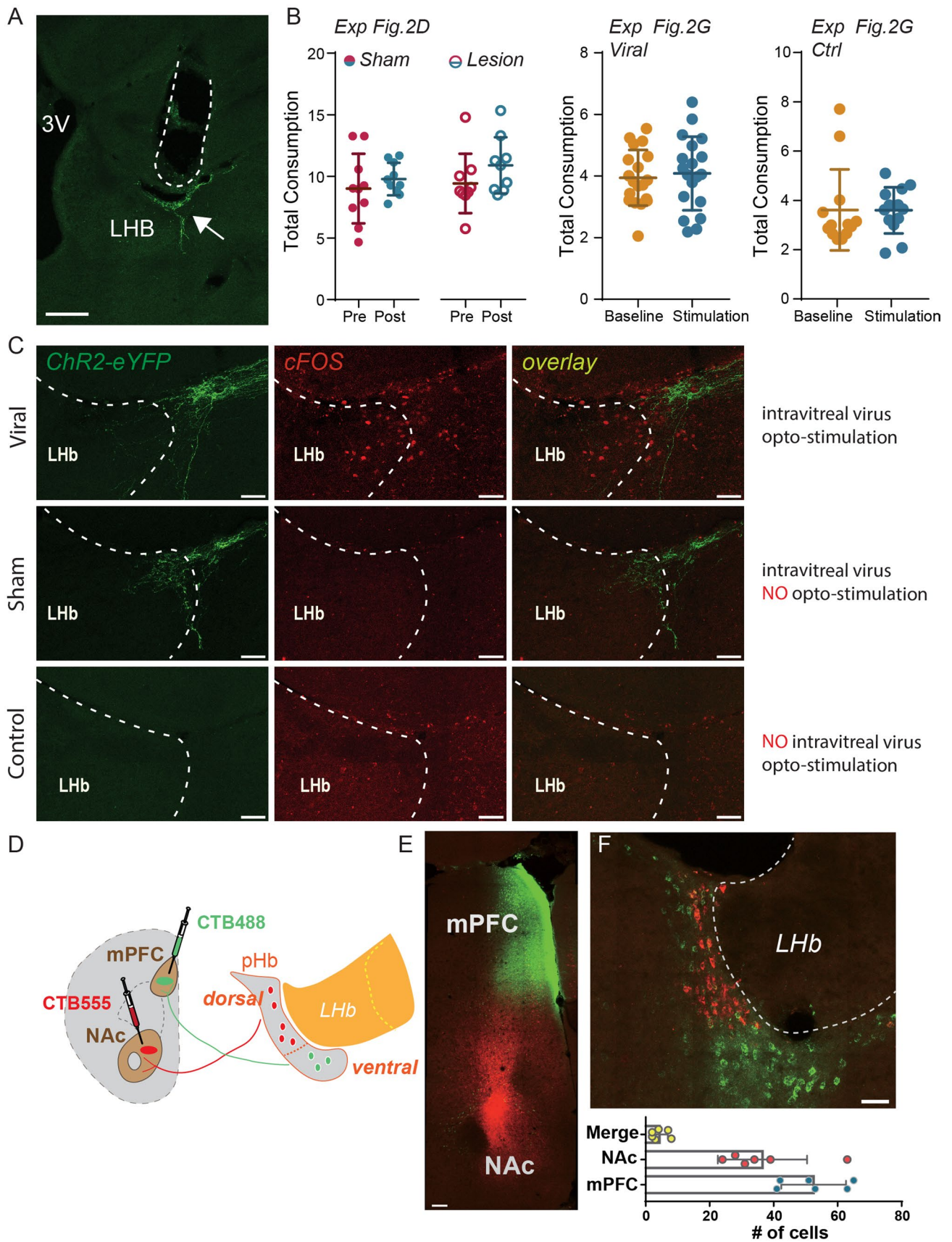


Extended Data Fig. 1 | See next page for caption.

**Extended Data Fig. 1 | Supporting information related to Fig. 1.** A) Immunostaining of Per1 in the SCN at different circadian times. Experiments were independently repeated 4 times for ZT 1 and 5, and 3 times for ZT 9, 13, 17, and 21. Scale: 50  $\mu\text{m}$ . B) Development of depressive-like behavior, as measured in the FST, during chronic exposure to LAN. The immobility time (mean  $\pm$  SD) progressively increased after 2 weeks (wks) under LAN conditions compared to the baseline before LAN treatment (Pre), and remained significantly elevated after 3 wks ( $n=8$  mice). Data obtained at 3 wks was plotted in Fig. 1. One-way ANOVA followed by Sidak's test:  $F(3, 28) = 5.3$ ,  $p=0.0051$ . Pre vs 3wks,  $p=0.0097$ ; Pre vs 4wks,  $p=0.0083$ . C-D) Persistence of 3wk LAN-induced depressive-like phenotype after 3wks, 6wks, and 9wks of recovery. LAN was given during the first 3 wks and removed afterwards. The immobility of LAN exposed animals ( $n=10$  mice) remained significantly higher than baseline at 6wks (or 3 wks of recovery), and returned to baseline level at 9-12 wks (or 6-9 wks of recovery, respectively). Repeated Measure One-way ANOVA with Tukey's test:  $F(1.99, 17.91) = 23.71$ ,  $p < 0.0001$ , Pre vs 3wks,  $p=0.0008$ ; Pre vs 6wks,  $p=0.0030$ ; 3wks vs 6wks,  $p=0.1162$ , ns; 3wks vs 9wks,  $p=0.0077$ ; 3wks vs 12wks,  $p=0.0005$ . Sucrose preference only recovered after 6wks (or 3wks of recovery). Repeat Measure One-way ANOVA with Tukey's test:  $F(1.63, 14.67)=15.96$ ,  $p=0.0004$ . Pre vs 3wks,  $p=0.0052$ ; 3wks vs 6wks,  $p=0.9034$ ; 3wks vs 9wks,  $p=0.1504$ ; 3wks vs 12wks,  $p=0.0003$ . E) Retinal projections to the pHb in WT and ipRGC-ablated animals. Retinal projections were visualized using intravitreally injected CTB-555. In WT animals, RGC terminals in the pHb were observed ( $n=3$  mice). Whereas in *Opn4-Cre::rosa-DTA* (DTA) animals, in which ipRGCs were ablated, retinal innervation to the pHb was completely eliminated ( $n=3$  mice). Scale: 100  $\mu\text{m}$ . F) Retinal innervations of the SCN in WT and ipRGC-ablated animals. RGC terminals within the SCN were visualized using intravitreally-administered CTB-555. In WT animals, typical dense innervation of the SCN was observed ( $n=3$  mice). In DTA animals, the retinal innervation of the SCN was substantially diminished but not completely eliminated ( $n=3$  mice). The scarce innervation may come from regular RGCs or few residual ipRGCs, and was likely adequate for normal photo-entrainment of DTA animals. Bar: 100  $\mu\text{m}$ . G) 3wks of LAN exposure did not affect overall locomotor activity level. Locomotor response to novelty (mean  $\pm$  SD) was assessed in an open field apparatus ( $n=10$  mice) before (pre) and after (post) 3wk LAN exposure, both during the light phase (D) or the dark phase (N). One-way ANOVA:  $F(2.482, 22.34) = 0.8581$ ,  $p=0.4586$ . H) The effect of LAN was examined using FST conducted at night in the dark. LAN exposure for 3 wks (post/blue, in comparison to the baseline (pre/pink) before LAN) induced an elevation of immobility (mean  $\pm$  SD) even when assessed during the dark phase.  $N=10$  mice,  $P=0.0002$ ,  $t=5.85$   $df=9$ , two-tailed paired t-test. I) Total water consumption (mean  $\pm$  SD) expressed as the ratio of total water consumption (water+sucrose) in SPT after LAN exposure (post) over that before LAN exposure (pre), corresponding to experiments in Figs. 1i, 1e, 1m, 1q, and 1u. None was significantly changed after LAN, with  $p$  values of 0.0532, 0.6930, 0.9683, 0.1770, and 0.0640, respectively, as determined by the two-tailed paired t-test comparing total consumptions pre vs. post within each group. \*\*:  $p < 0.01$ ; \*\*\*:  $p < 0.001$ .

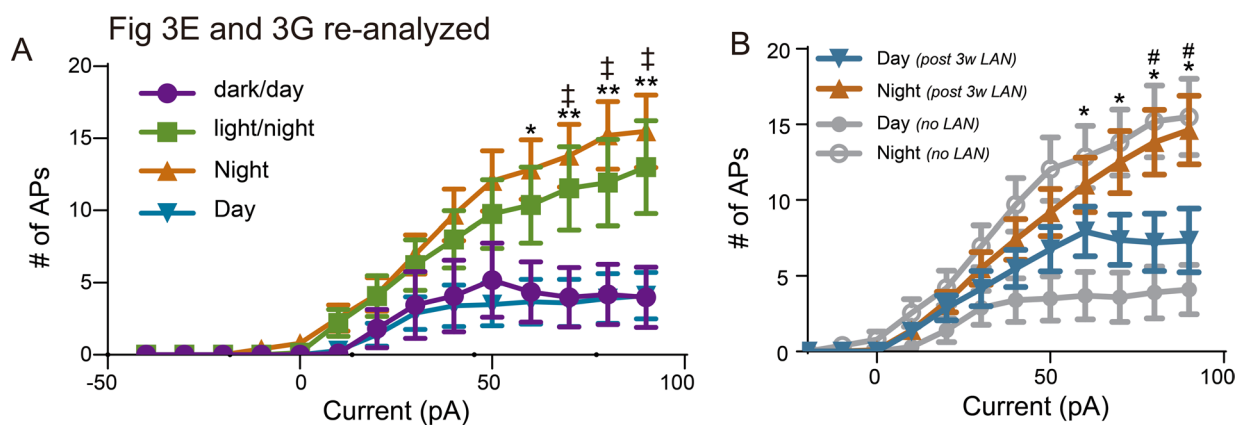


**Extended Data Fig. 2 | Supporting information related to Fig. 2.** A) Schematic diagram of anterograde tracing with intravitreally-injected tracers. B) Retinal projections to the pHb area revealed by intravitreally-injected CTB-555 (b') and HSV (b''), and ipRGC projections to the pHb revealed by AAV2-DIO-Channelrhodopsin (ChR2)-eYFP administered in Opn4-Cre mice (b'''). All tracing experiments were repeated at least three times. Scale: 100  $\mu$ m. C) Schematic diagram of retrograde tracing from the pHb to retina. D) Retrogradely labeled (CTB, red) M1 ipRGCs (melanopsin), with dendrites stratified solely in the OFF sublamina of the retinal inner plexiform layer. Scale: 25  $\mu$ m. E) Quantification of retrograde tracing results (contra: eye contralateral to the injection side; ipsi: ipsilateral eye; CTB: CTB only; Mela: CTB/melanopsin co-stained; n = 5 mice; contra: 18 cells; ipsi: 7 cells; Contra/mela: 75 cells; ipsi/mela: 6 cells). F) Subtype analysis of pHb-projecting ipRGCs judged from the stratification pattern (data were pooled from 4 retinae due to the difficulty of finding clearly stained dendrites and the cell body to which they belong on the same section. M1: 22 cells; M2: 2 cells; M3: 4 cells; Dislocated (DL): 2 cells). G) Fluorescence from CTB-555 at the injection site (pHb). Scale: 100  $\mu$ m. H) Example of a M2 ipRGC that was stratified (arrowhead) in the ON sublamina of the retinal inner plexiform layer (IPL). Scale: 25  $\mu$ m. I) Example of a M3 ipRGC that was stratified in both ON and OFF layers (arrowheads). Scale: 25  $\mu$ m. J) Example of a dislocated ipRGC that appeared on the amacrine cell layer. Experiments in G-I were independently repeated four times in two mice. Scale: 25  $\mu$ m.

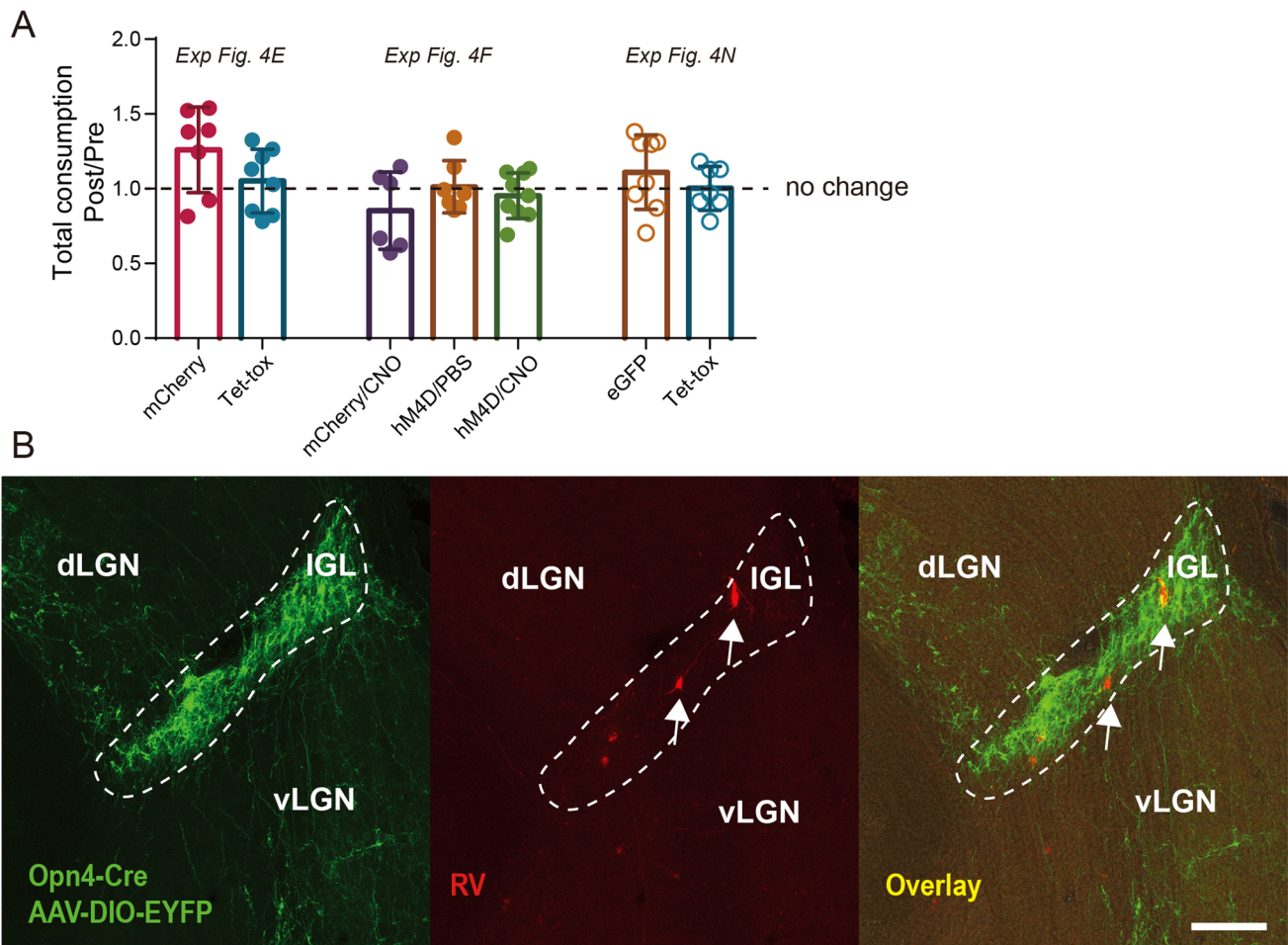


Extended Data Fig. 3 | See next page for caption.

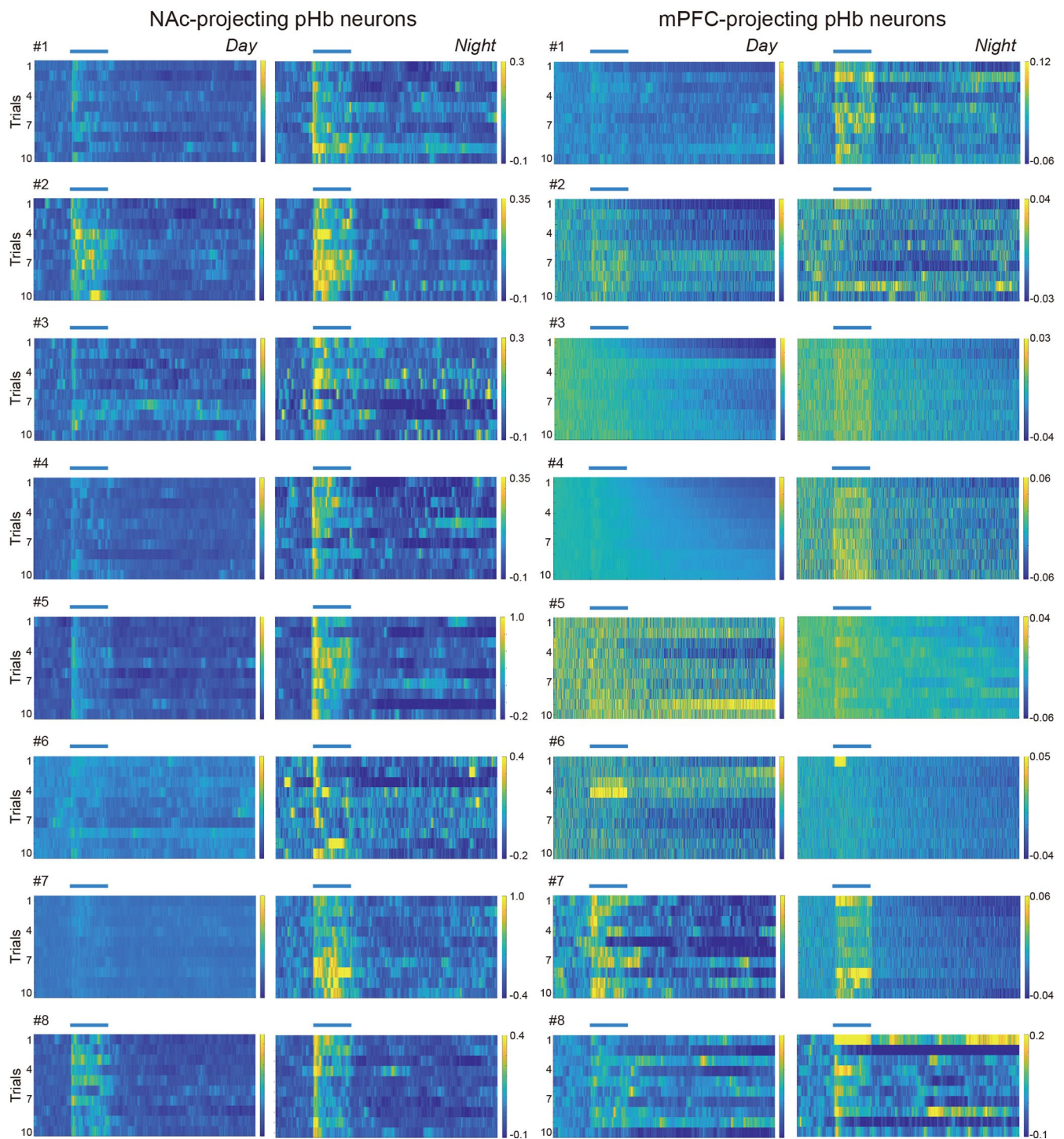
**Extended Data Fig. 3 | Additional supporting information related to Fig. 2.** A) Histology for the optogenetic experiments in Fig. 2g–2i. Scale: 200  $\mu\text{m}$ . B) Total water consumption (in grams/g, expressed as mean  $\pm$  SD) corresponding to experiments in Figs. 2d and 2g, with p values of 0.4896, 0.2337, 0.7212, and 0.9695, for the sham (n=10 mice), lesion (n=9 mice), viral (n=19 mice), and ctrl (n=13 mice) groups, respectively, as determined by two-sided paired t-test. C) Upregulation of cFos in the pHb elicited by the optostimulation of ipRGC terminals. Expression of cFos was induced by optostimulation of ipRGCs axonal terminals within the pHb. Selective expression of ChR2 in ipRGCs was achieved via intravitreal injection of AAV2/2-EF1 $\alpha$ -DIO-ChR2-eYFP in Opn4-Cre mice (n=5 sections). In sham-treated mice (littermates that received virus injection but no local opto-stimulation), minimum expression of cFos was observed (n=6 sections). Parallel treated control mice in which virus injection was omitted did not respond to local optostimulation with elevated cFos expression (n=7 sections). Bars: 50  $\mu\text{m}$ . D) Schematic diagram of simultaneous retrograde tracing from NAc and mPFC using CTB-555 and CTB-488, respectively. E) Fluorescence at the injection sites: mPFC (green) and NAc (red). Experiments were independently repeated six times. Scale: 150  $\mu\text{m}$ . F) Retrogradely-labelled NAc-projecting dpHb neurons (red dots) and mPFC-projecting vpHb neurons (blue dots) with rare overlaps (yellow dots). n=6 mice. Data were expressed as mean  $\pm$  SD. Scale: 100  $\mu\text{m}$ .



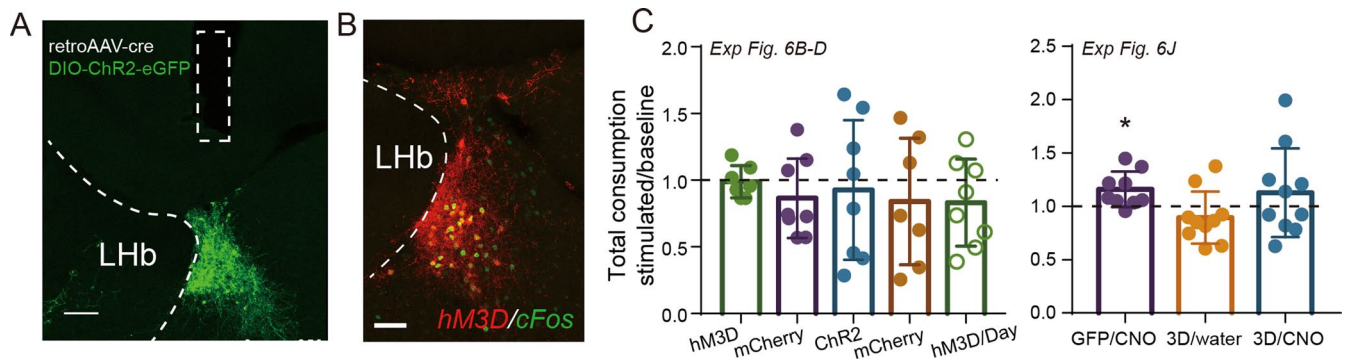
**Extended Data Fig. 4 | Nested analysis of data presented in Figs. 3e and 3g.** A) Data presented in Fig. 3e were re-analyzed using nested ANOVA. Quantification of action potentials (mean  $\pm$  SEM) generated by current injections in NAc-projecting dpHb neurons (Day:  $n=10$  neurons from 3 mice; Night:  $n=20$  neurons from 5 mice; Dark/day: 11 neurons from 4 mice; Light/night: 13 neurons from 4 mice). Nested ANOVA with Tukey's test revealed significant difference among groups at: 60 pA:  $p=0.0111$ ,  $F(3,50)=4.104$  (\*); 70 pA:  $p=0.0050$ ,  $F(3,50)=4.825$  (\*\*); 80 pA:  $p=0.0034$ ,  $F(3,50)=5.176$  (\*\*); 90 pA:  $p=0.0027$ ,  $F(3,50)=5.391$  (\*\*); ‡: "Day" significantly different from "Night" and "Light/night" significantly different from "dark/day". B) Data presented in Fig. 3g were re-analyzed using nested two-sided t-test. Circadian variations in the intrinsic excitability of NAc-projecting dpHb neurons after 3 wk LAN exposure.  $n=18$  neurons from 4 mice for "Day (post 3w LAN)" and 22 neurons from 5 mice for "night (post 3w LAN)". Data were plotted as mean  $\pm$  SEM. #: Significant difference determined by nested t-test at 80 pA ( $p=0.0296$ ;  $t=2.260$ ,  $df=38$ ) and 90 pA ( $p=0.0258$ ,  $t=2.320$ ,  $df=38$ ). Data of "Day (no LAN)" and "Night (no LAN)" were replotted from A in light gray for easy comparison. Difference between Day (no LAN) and Night (no LAN) was annotated by \*.



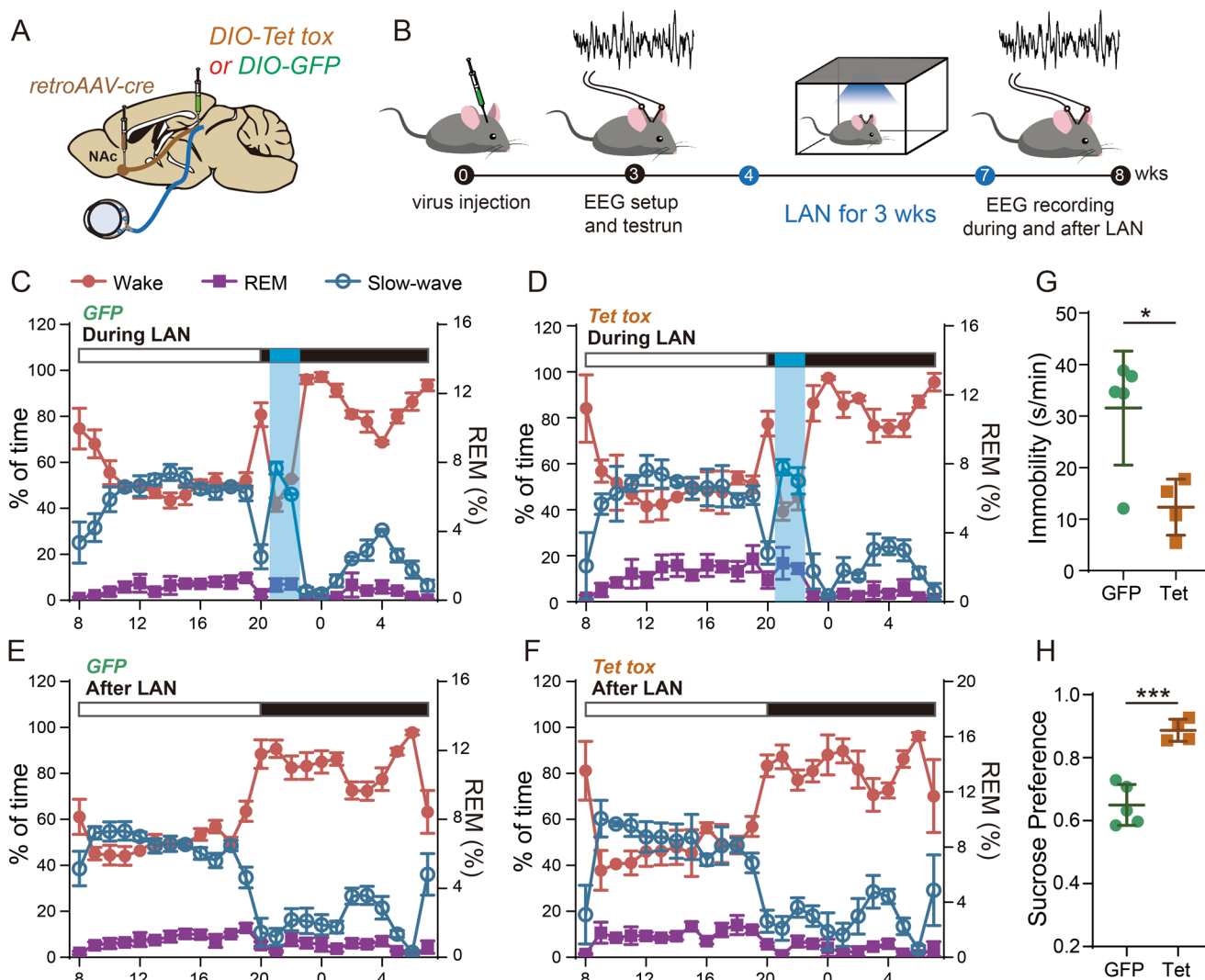
**Extended Data Fig. 5 | Supporting information related to Figs. 4–5.** A) Changes in total water consumption (mean  $\pm$  SD) expressed as the ratio of the total water volume (water+sucrose) in the SPT after LAN exposure to that before LAN exposure, corresponding to experiments in 4e ( $n=7$  mice for mCherry and  $n=8$  mice for Tet-tox), 4f ( $n=6$  mice for mCherry/CNO,  $n=7$  mice for hM4D/PBS, and  $n=9$  mice for hM4D/CNO), and 4n ( $n=9$  mice for eGFP and  $n=7$  mice for Tet-tox). None was significantly altered by LAN exposure with  $p$  values of 0.0583, 0.6833, 0.1663, 0.9858, 0.3895, 0.2829, and 0.9468, respectively, as determined by two-tailed paired  $t$ -test comparing total consumptions pre vs. post within each group. B) (Related to experiments in Fig. 5a–d) Retrograde trans-synaptic tracing with RV revealed presynaptic inputs from IGL to NAc-projecting pHb neurons. The inter-geniculate leaflet (IGL, outlined) was densely innervated by ipRGCs. AAV2/2-EF1 $\alpha$ -DIO-ChR2-eYFP was intravitreally injected to selectively express eYFP in ipRGCs, and intense labeling within the IGL was observed. dLGN: dorsal lateral geniculate nucleus. vLGN: ventral lateral geniculate nucleus. RV-labeled cells (arrowheads) were observed in the IGL. On average  $26 \pm 22$  IGL neurons were observed on each side of each animal from a total of 6 mice. Bar: 100  $\mu$ m.



**Extended Data Fig. 6 | Heat-maps for the photometric experiments in Fig. 5.** Heat-maps showing the day/night responses of all 16 clusters (8 NAc-projecting dpHb neuron clusters and 8 mPFC-projecting vpHb neuron clusters) in the photometry experiments. Within the same pair (day vs. night), heat-maps were drawn on the same color-scale for a clearer comparison between day and night responses. Across different pairs, the scales were different as marked on the side.



**Extended Data Fig. 7 | Supporting information related to Fig. 6.** A) Histology for the optogenetic manipulation of the dpHb-NAc projection in experiment 6d, e, f, and h. Trace of the optic fiber was outlined by the dotted line. Verification was independently performed 8 times. Scale: 100  $\mu$ m. B) Histology showing NAc-projecting dpHb neurons expressing hM3D (red) and cFos (green) after i.p. injection of 1 mg/kg CNO, corresponding to experiments 6b, c, and g. Experiments were independently performed nine times. Scale: 100  $\mu$ m. C) Changes in the total water consumption (mean  $\pm$  SD) expressed as the ratio of the total water volume (water+sucrose) in the SPT after various stimulations (chemogenetic, optogenetic, or chronic CNO) to that during baseline period. Corresponding to experiments in Fig. 6b: n = 7 mice for hM3D,  $p = 0.6721$ ; n = 8 mice for mCherry,  $p = 0.2153$ . Corresponding to experiments in Fig. 6c, n = 8 mice for hM3D/Day,  $p = 0.1846$ . Corresponding to experiments in Fig. 6d, n = 8 mice for ChR2,  $p = 0.3375$ ; n = 7 mice for mCherry,  $p = 0.3517$ , all determined by the two-tailed paired t-test comparing total consumptions pre vs. post within each group, indicating no change before vs. after stimulations. Corresponding to experiments in Fig. 6j, n = 10 mice for GFP/CNO,  $p = 0.0204$  (\*); n = 10 mice for 3D/water,  $p = 0.1327$ ; and n = 10 mice for 3D/CNO,  $p = 0.5638$ , all determined by the two-tailed paired t-test comparing total consumptions pre vs. post within each group, indicating a slight increase of total water consumption in the GFP/CNO group after CNO administration. \*:  $p < 0.05$ .



**Extended Data Fig. 8 | EEG recordings of mice during and after LAN exposure.** A) Diagram of strategy for inhibitory manipulation of the dpHb-NAc projection. Mice were randomly allocated to receiving injections of either DIO-Tet-tox (experimental group) or DIO-GFP (control group) into the pHb area. B) Experimental procedures for the EEG recordings during and after LAN exposure. Animals were allowed to recover for 3wks after stereotaxic injections of the viruses to ensure adequate habituation as well as virus expression, followed by EEG setup including electrode implantation and test runs. EEG was recorded during the last several days of LAN, after the termination of LAN exposure. C-D) Sleep-wake architecture of animals during LAN exposure. For both GFP (C,  $n=3$  mice) and Tet-tox (D,  $n=3$  mice) groups, the presence of light during the dark phase elevated the percentage of slow-wave sleep (blue open circle, mean  $\pm$  SEM) and REM sleep (purple square, plotted to the right Y axis, mean  $\pm$  SEM) but suppressed wakefulness (orange circle, mean  $\pm$  SEM) in both GFP and Tet-tox mice. E-F) Both GFP and Tet-tox animals ( $n=3$  mice in each group) resumed normal sleep-wake architecture after the termination of 3wk LAN exposure. Data were expressed as mean  $\pm$  SEM. G) FST of GFP and Tet-tox animals after LAN treatment. GFP mice ( $n=5$  mice, green) exhibited significantly higher immobility (mean  $\pm$  SD) than Tet-tox animals ( $n=4$  mice, brown).  $p=0.0142$ ,  $t=3.407$   $df=6.046$ , two-sided unpaired t-test with Welch's correction. H) Sucrose preference (mean  $\pm$  SD) of GFP mice was statistically lower than Tet-tox mice.  $p=0.0003$ ,  $t=6.993$   $df=6.344$ , two-sided unpaired t-test with Welch's correction. \*:  $p < 0.05$ ; \*\*\*:  $p < 0.001$ .

## Reporting Summary

Nature Research wishes to improve the reproducibility of the work that we publish. This form provides structure for consistency and transparency in reporting. For further information on Nature Research policies, see [Authors & Referees](#) and the [Editorial Policy Checklist](#).

### Statistics

For all statistical analyses, confirm that the following items are present in the figure legend, table legend, main text, or Methods section.

n/a Confirmed

- The exact sample size ( $n$ ) for each experimental group/condition, given as a discrete number and unit of measurement
- A statement on whether measurements were taken from distinct samples or whether the same sample was measured repeatedly
- The statistical test(s) used AND whether they are one- or two-sided  
*Only common tests should be described solely by name; describe more complex techniques in the Methods section.*
- A description of all covariates tested
- A description of any assumptions or corrections, such as tests of normality and adjustment for multiple comparisons
- A full description of the statistical parameters including central tendency (e.g. means) or other basic estimates (e.g. regression coefficient) AND variation (e.g. standard deviation) or associated estimates of uncertainty (e.g. confidence intervals)
- For null hypothesis testing, the test statistic (e.g.  $F$ ,  $t$ ,  $r$ ) with confidence intervals, effect sizes, degrees of freedom and  $P$  value noted  
*Give  $P$  values as exact values whenever suitable.*
- For Bayesian analysis, information on the choice of priors and Markov chain Monte Carlo settings
- For hierarchical and complex designs, identification of the appropriate level for tests and full reporting of outcomes
- Estimates of effect sizes (e.g. Cohen's  $d$ , Pearson's  $r$ ), indicating how they were calculated

*Our web collection on [statistics for biologists](#) contains articles on many of the points above.*

### Software and code

Policy information about [availability of computer code](#)

Data collection

Electrophysiological data were collected using Axon pClamp software (Molecular Devices)(vision 9.2). Photometric data were collected using the THINKERTECH fiber photometry recording system. EEG data were collected using SleepSign3-OBI(vision 2.0)

Data analysis

Axon clampfit software (molecular Devices) was used to analyze electrophysiological data. ImageJ(vision 1.51j8) was used for image processing. A customized script written in MATLAB(vision 2017b) was used to analyze photometric data. Behavioral data were counted off-line by investigators, except for RTPA, in which Ethovision(vision 8.5) was used to generate preference scores. SleepSign3-OBI(vision 2.0) was used to analyze EEG data.

For manuscripts utilizing custom algorithms or software that are central to the research but not yet described in published literature, software must be made available to editors/reviewers. We strongly encourage code deposition in a community repository (e.g. GitHub). See the Nature Research [guidelines for submitting code & software](#) for further information.

### Data

Policy information about [availability of data](#)

All manuscripts must include a [data availability statement](#). This statement should provide the following information, where applicable:

- Accession codes, unique identifiers, or web links for publicly available datasets
- A list of figures that have associated raw data
- A description of any restrictions on data availability

The data that support the findings of this study, besides what has been included in this manuscript (including the supporting information), are available from the corresponding author upon request.

## Field-specific reporting

Please select the one below that is the best fit for your research. If you are not sure, read the appropriate sections before making your selection.

Life sciences       Behavioural & social sciences       Ecological, evolutionary & environmental sciences

For a reference copy of the document with all sections, see [nature.com/documents/nr-reporting-summary-flat.pdf](https://www.nature.com/documents/nr-reporting-summary-flat.pdf)

## Life sciences study design

All studies must disclose on these points even when the disclosure is negative.

Sample size	No statistical methods were used to pre-determine sample sizes. Sample sizes were indicated in the figures and associated text, and similar to those reported in previous studies (Menard et al. 2017, Nature Neuroscience; Ramirez et al. 2015, Nature; Yao et al. 2018, Nature Neuroscience).
Data exclusions	For all electrophysiological experiments, cells that appeared unhealthy (input resistance lower than 150 MΩ, or resting membrane potential positive than -40mV) or without adequate access (access resistance higher than 30 MΩ, or initial AP not reaching +20 mV) were excluded from data analysis. Those are typical and well established criteria widely employed in patch-clamp experiments to ensure quality of the recording. In the forced swimming test, one animal in Fig. 4C and one in Fig. 6G with extreme basal levels (0 s immobility time at baseline) were excluded from further experiments. The average immobility time of naive/WT animals was consistently around 20 s in our experience, thus a 0 s basal level might indicate an abnormal locomotor status or anxiety-like emotional state of the animal, which may interfere with the interpretation of the results. Therefore, no further experiment was performed on these animals. In the photometric experiments, 6 recording sites from 6 animals (NAc) and 4 recording sites from 3 animals (mPFC) were excluded from final analysis due to unsatisfactory expression of viruses (fewer than ten cells) or incorrect placement of the optical fiber (located outside the pHb area and the vicinity above the pHb). Adequate expression of GCAMP and correction orientation of the optical fiber are critical for obtaining reliable photometric data, and are pre-established criteria in all published work involving photometric experiments. For EEG recordings, one animal died during habituation and two were excluded due to high noise level in the recordings. For long-term EEG recordings in freely-moving animals, movement of the animals could occasionally cause large noises in the signal, which would make accurate sleep-wake scoring impossible. Thus, samples with large and frequent noises were excluded from analysis. For the pHb lesion experiment, data of one animal was removed from the NMDA lesion group due to incomplete lesion revealed by the post-hoc verification using GFAP staining. For electrophysiological experiments on the dpHb-NAc neurotransmission, neurons that receive polysynaptic inputs or unstable inputs were not further pursued using pre-established criteria.
Replication	Each experiment was repeated at least three times. All replications were conducted successfully except for post-hoc verification such as the GFAP staining in lesion experiments. The samples that failed quality control assessments (e.g incomplete lesion) would be removed from further analysis.
Randomization	For experiments involving various treatments, littermates were randomly assigned to experimental and control groups. In any specific experiment, animals were examined in a semi-randomized order, with alternate control and experimental animals.
Blinding	The experimenters who collected the data were not blind to the group assignment of the object. However, data were analyzed either by automated software using consistent parameters, or by investigators who were blind to the experimental conditions.

## Reporting for specific materials, systems and methods

We require information from authors about some types of materials, experimental systems and methods used in many studies. Here, indicate whether each material, system or method listed is relevant to your study. If you are not sure if a list item applies to your research, read the appropriate section before selecting a response.

### Materials & experimental systems

n/a	Involved in the study
<input type="checkbox"/>	<input checked="" type="checkbox"/> Antibodies
<input checked="" type="checkbox"/>	<input type="checkbox"/> Eukaryotic cell lines
<input checked="" type="checkbox"/>	<input type="checkbox"/> Palaeontology
<input type="checkbox"/>	<input checked="" type="checkbox"/> Animals and other organisms
<input checked="" type="checkbox"/>	<input type="checkbox"/> Human research participants
<input checked="" type="checkbox"/>	<input type="checkbox"/> Clinical data

### Methods

n/a	Involved in the study
<input checked="" type="checkbox"/>	<input type="checkbox"/> ChIP-seq
<input checked="" type="checkbox"/>	<input type="checkbox"/> Flow cytometry
<input checked="" type="checkbox"/>	<input type="checkbox"/> MRI-based neuroimaging

## Antibodies

### Antibodies used

Primary antibodies used in the present study are as follows:  
 Rabbit anti-GABA (Sigma-Aldrich catalog: A2052; lot# 018M4808V; polyclonal; dilution:1:500; RRID: AB\_477652);  
 Rabbit anti-Glutamate (Sigma-Aldrich catalog: G6642; lot# 108M4860V; polyclonal; dilution:1:500; RRID: AB\_259946);  
 Rabbit anti-GFAP (Sangon Biotech catalog: D120691; polyclonal; dilution:1:200);  
 Rabbit anti-c-fos (Synaptic Systems catalog: 226003; lot# 7-78; polyclonal; dilution:1:5000; RRID: AB\_2231974);

Rabbit anti-melanopsin (Advanced Targeting System, catalog: AB-N38; lot# 112-16; polyclonal; dilution:1: 10000; RRID: AB\_1266797);

Rabbit anti-per1 (Abcam catalog: ab136451, lot# GR3216520-2; polyclonal; dilution:1:500).

Secondary antibodies used in the present study are as follows:

Alexa Fluor 568 (Thermo Fisher catalog: A-11036 lot# 2155282; polyclonal; dilution:1:500; RRID: AB\_10563566)

Alexa Fluor 488 (Thermo Fisher catalog: A-11034 lot# 2069632; polyclonal; dilution:1:500; RRID: AB\_2576217).

## Validation

Antibodies used in the study were commercially available and validated by the manufacturers.

anti-GABA(Target: Rat, mouse, rabbit, guinea pig and lizard; Application: IHC;WB;Dot; reference article: PMID 16207866; more relevant papers on <https://www.sigmaaldrich.com/catalog/product/sigma/a2052?lang=en&region=US>)

anti-Glutamate(Target: wide range; Application: IHC;WB;Dot; reference article: PMID 20921396; more relevant papers on <https://www.sigmaaldrich.com/catalog/product/sigma/g6642?lang=en&region=US>)

anti-GFAP(Target: Human, Mouse, Rat; Application: ELISA, IHC;more relevant info on <https://www.sangon.com/productDetail?productInfo.code=D120691>)

anti-c-fos(Target: human,ra,mouse ,monkey, ape, cow, dog, pig; Application: WB,ICC,IHC,IHC-P/FFPE,IP; reference article: PMID 32170133; more relevant papers on <https://www.sysy.com/products/c-fos/facts-226003.php>)

anti-melanopsin(Target: mouse; Application: IHC; eg PMID 30587542 <https://atsbio.com/products/abn38/>)

anti-per1(Target: Mouse, Rat, Human; Application:WB,IHC; reference article: PMID 31030999; more relevant papers on <https://www.abcam.cn/per1-antibody-n-terminal-ab136451.html>)

Alexa Fluor 568(Target: Rabbit; Application: ICC,IF,IHC(F)IHC,IHC(P),IHC(Free),Misc,WB; reference article: PMID 27897178; more relevant papers on <https://www.thermofisher.com/cn/zh/antibody/product/Goat-anti-Rabbit-IgG-H-L-Highly-Cross-Adsorbed-Secondary-Antibody-Polyclonal/A-11036>)

Alexa Fluor 488(Target: Rabbit; Application: ICC,IF,IHC(F)IHC,IHC(P),IHC(Free),Misc,WB; reference article: PMID 28102238; more relevant papers on <https://www.thermofisher.com/cn/zh/antibody/product/Goat-anti-Rabbit-IgG-H-L-Highly-Cross-Adsorbed-Secondary-Antibody-Polyclonal/A-11034>)

## Animals and other organisms

Policy information about [studies involving animals](#); [ARRIVE guidelines](#) recommended for reporting animal research

### Laboratory animals

Adult mice (2–4 month old, male and female C57BL/6 or transgenic mice as specified) were housed at a constant temperature with ad libitum access to standard rodent diet under 8am–8pm 12 h:12 h light/dark cycle (~200 lux white ambient illumination) except for during LAN exposure (~400 lux blue illumination between 21:00–23:00). All wild-type mice used in this study were obtained from the Model Animal Research Center of Nanjing University. rd1/cDTA/Opn4<sup>-/-</sup> and Opn4-Cre mouse were general gifts from Dr. King-Wai Yau at Johns Hopkins University. Rosa-DTA mouse were provided by Dr. Xiao Yu at Shandong University.

### Wild animals

This study did not involve wild animals

### Field-collected samples

This study did not involve field-collected samples

### Ethics oversight

Institutional Animal Care and Use Committees at the University of Science and Technology of China (USTC) and the Chinese Academy of Sciences (CAS).

Note that full information on the approval of the study protocol must also be provided in the manuscript.